On the Stress Analysis and the Stability Computation of Earth Embankments. Part I Stress Distribution in Earth Embankments

AUTHOR(S):

AKAI, Koichi

CITATION:

AKAI, Koichi. On the Stress Analysis and the Stability Computation of Earth Embankments. Part I Stress Distribution in Earth Embankments. Bulletins - Disaster Prevention Research Institute, Kyoto University 1957, 17: 1-25

ISSUE DATE:

1957-03-25

URL:

http://hdl.handle.net/2433/123671

DISASTER PREVENTION RESEARCH INSTITUTE
BULLETIN No. 17 MARCH, 1957

ON THE STRESS ANALYSIS AND THE STABILITY COMPUTATION OF EARTH EMBANKMENTS

BY

KŌICHI AKAI

KYOTO UNIVERSITY, KYOTO, JAPAN

DISASTER PREVENTION RESEARCH INSTITUTE
KYOTO UNIVERSITY
BULLETINS

Bulletin No. 17 March, 1957

On the Stress Analysis and the Stability Computation of Earth Embankments

By

Kōichi AKAI

Contents

Synopsis

As the fundamental research for the stability analysis in the embankment design, the stress distribution and the character of pore pressures in earth embankments are investigated in this paper. In the author's stability analysis, the residual strength reserved in the embankment at the natural state is estimated, and then the externally applied forces and the internally acting pore pressures are computed. Thus, the stability of the earth embankment is checked by comparing these forces with each other.

Part I is described concerning the stress distribution in earth embankments. First, scrutinizing several conventional studies ever presented, it is pointed out that there exist some inaccuracies or contradictions in the substantial problem of determining the stability of the structure, although they have the remarkable importance partially. Then, in order to modify these inconsistencies and to develop their substances, the author introduces the concept of the residual strength in the embankment and designates the stress distribution at rest as the function of compaction. Therefore, the coefficient of earth pressure at rest or of compaction is treated as a factor of importance to estimate the stress distribution in this analytical solution.

The character of pore pressures in earth embankments is studied in Part II, to investigate their effects on the stability of the structure. In this part of the paper, stability analyses during the fill construction and for rapid-drawdown of the reservoir are described, illustrating some numerical calculations, respectively. The failure of the earth embankment due to these pore pressures is still considered as progressive one. In the result, it is shown that such pore pressures have a serious effect on the stability of the earth embankment, whereupon the method of reasonable design should be established.

Part I Stress Distribution in Earth Embankments

1. Introduction

In the stress analysis in the earth embankment having a considerable length, the phenomenon can be treated as a plane-strain problem in the plane perpendicular to the axis of the embankment. Many studies have been presented concerning such a kind of analysis, and some of them are remarkable ones which are deduced under the consideration of mechanical properties of soil in the actual embankment. In general, however, analytical methods of stress using the theory of elasticity have been very controversial against their application and obliged to make large modifications[1]. Accordingly, common analyses are performed using the condition for plastic equilibrium of soil constituting the earth embankment, besides two equations of stress equilibrium of soil element respecting the two-dimensional stress components in the embankment. As this condition is reperesented in the form of the equation of second order respecting to the stress components, two solutions are obtained, corresponding to the active and passive limiting states, and there may be the stress distribution of the actual state between these two solutions.

In the present part of this paper, the author introduces the equation of the residual strength in the embankment, instead of the condition for plastic equilibrium. The failure of the earth embankment is, therefore, considered as a progressive one caused by the encroachment on the reserve strength in the embankment, with the increase of the shearing stress by external forces acting on it. Then, using the equation of stress equilibrium at rest in terms of the coefficient of compaction of the embankment material, a calculating method is proposed to obtain the solution of stress distribution in earth embankments corresponding to the arbitrary degree of compaction, and the result is compared with the experimental study with sand models.

2. Scrutiny of Conventional Studies

(1) Anzo's method and Jonson's method.

The analytical method of stress in the wedge-shaped embankment made of the granular material which has been presented by Anzo[2] has an interesting

originality in such a point, that he has introduced a concept of "influenced region" and of "influenced angles" According to his method, some assumptions were skillfully made that the influenced region is composed of many small elementary wedges as shown in Fig. 1, in each of which the stress variation may be expressed by the linear functions of x and y, and that at the limiting state of the equilibrium the maximum obliquity of stress at the point on divided boundaries becomes equal to the angle of internal friction of the material.

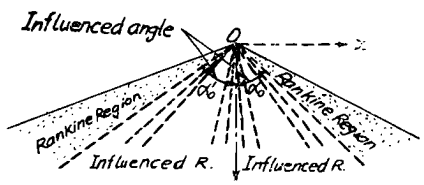

Fig. 1 Rankine regions and the influenced region of embankment in Anzo's mothod.

The stress function and the stress components in this analysis are expressed in the following form, when the tensile stresses are taken as positive sign, for each elementary wedges in Fig. 1 :

$$\left.\begin{aligned} \chi_i &= \gamma_s\left(\frac{A_i x^3}{6}+\frac{B_i x^2 y}{2}+\frac{C_i x y^2}{2}+\frac{D_i y^3}{6}\right),\\ [\sigma_y]_i &= \frac{\partial^2 \chi_i}{\partial x^2}-\gamma_s y=\gamma_s[A_i x+(B_i-1)y],\\ [\tau_{xy}]_i &= -\frac{\partial^2 \chi_i}{\partial x \partial y}=-\gamma_s[B_i x+C_i y],\\ [\sigma_x]_i &= \frac{\partial^2 \chi_i}{\partial y^2}=\gamma_s[C_i x+D_i y], \end{aligned}\right\} \quad \cdots\cdots\cdots\cdots(1)$$

where γ_s is the unit weight of the earth material and A_i, B_i, C_i, D_i are the coefficients having constant values in each wedges, respectively. These coefficients are determined from the condition of stress continuity and of plastic equilibrium of the embankment material on each divided boundaries, the latter being written in the following equation.

$$\{[\sigma_y]_i-[\sigma_x]_i\}^2+4[\tau_{xy}]_i^2=\sin^2\varphi\{[\sigma_y]_i+[\sigma_x]_i\}^2, \quad \cdots\cdots\cdots\cdots(2)$$

where φ is the angle of internal friction of the material.

Solving the above equations in accordance with the boundary conditions, the influenced angle α_0 is given in the following form :

$$\left.\begin{aligned} &\text{For the active state :} \quad \alpha_0=\frac{\pi}{4}-\frac{\varphi}{2}-\phi,\\ &\text{For the passive state :} \quad \alpha_0=\frac{\pi}{4}+\frac{\varphi}{2}-\phi', \end{aligned}\right\} \quad \cdots\cdots\cdots\cdots(3)$$

wherein ψ or ψ' is the angle of the axis of stress ellipse in the outest Rankine region to the vertical line, and is shown as follows :

$$\tan 2\psi \text{ or } \tan 2\psi' = -\frac{2[\tau_{xy}]_R}{[\sigma_y]_R - [\sigma_x]_R}. \qquad \cdots\cdots\cdots\cdots\cdots\cdots(4)$$

in which, suffix R is referred to Rankine region.

In the above Anzo's method, although the more number of the division of region is taken, the higher the precision of the analysis becomes, it is very tedious to solve the simultaneous equation, because the number of boundary conditions also increases proportionally.

Jonson[3] has made an analysis using the polar co-ordinate for the similar problem. In his method, it seems to be somewhat rough theoretically, because he did not consider the distinction between the "Rankine region" and the "influenced region", but he considered an embankment as a whole. But this is an analytical method of progressive approximation as well as Anzo's one in the same idea, that the condition for plastic equilibrium should be satisfied on several lines passing the crest of the embankment.

In these two methods, two equations of stress equilibrium of soil element in the direction of the axis of co-ordinates and a condition for plastic equilibrium of soil mass were used in order to determine the stress components σ_x, σ_y, τ_{xy} or σ_r, σ_θ, $\tau_{r\vartheta}$. As this condition is, however, written in the form of Eq. (2) for cohesionless soils, two limiting values corresponding to the active and passive states are computed as the stress components, and there is a destined contradiction that the embankment should collapse as a whole at these limiting states of equilibrium.

The cause of this contradiction consists in a constraint that Eq. (2) should be satisfied at every point in the embankment. As is already described, the more number of lines passing the crest on which Eq. (2) is held is taken, the higher the precision of these analyses becomes, but this means that the degree of constraint is increasing at the same time, whereas a collapse of the actual embankment will never take place at once everywhere. It is more rational to consider that the greater part of an embankment remains in the natural state even when the limiting state of plastic equilibrium has been reached partly, and that this partial limiting state will spread over the other part of natural state progressively.

(2) Glover-Cornwell's method.

Glover and Cornwell[4] are the first introducers of this idea for earth embankments. In the solution of their analytical method, adding to two equations of stress equilibrium, it is required that the stresses satisfy the following compatibility equation in those regions where the relation between stresses is such as will not permit grains to change their relative positions (i. e. in "elastic region") :

$$\frac{\partial^2\sigma_y}{\partial x^2}+\frac{\partial^2\sigma_x}{\partial y^2}-2\frac{\partial^2\tau_{xy}}{\partial x\partial y}=0, \qquad \cdots\cdots\cdots\cdots\cdots(5)$$

and in the regions where this condition is not met, it is assumed that the relation between the principal stresses is such as to make slippage imminent on the planes of least resistance (i. e. in "plastic region"). Defining the "reserve strength"

$$R=C+\sigma_n\tan\varphi-\tau, \qquad \cdots\cdots\cdots\cdots\cdots(6)$$

they distinguished an embankment into two kinds, one of which is the "plastic region" where $R=0$, and another is the "elastic region" where $R\neq 0$. In the former region Eq. (2) should be held for cohesionless soils, and in the latter Eq. (5) will be applicable by their definition. The division of an embankment into elastic and plastic regions offers an interesting approach to the analytical problem, and the concept of the reserve strength R is valuable. But they divided these regions too mechanically, and did not prove as to establish the compatibility equation (5) in the elastic region. Moreover they found Rankine's state of stress in the plastic region, whereas the truth would be a natural state with "at rest" presssure as Benscoter[5] pointed out in his discussion.

The following conclusion is obtained, precisely comparing Glover-Cornwell's method with Anzo's one already mentioned, that in the regional sense of division, the "plastic" and "elastic" regions in the former are nothing else but the "Rankine region" and the "influenced region" in the latter, respectively. And so the difference between these two analytical methods consists in a point, that Anzo divided the influenced region into many elementary wedges by the straight lines passing the crest of the embankment, and made an effort to satisfy the condition for plastic equilibrium Eq. (2) in each divided wedges, whereas Glover-Cornwell did not make such divisions. Consequently, as Krynine[6] discussed, as soon as the stresses at the boundaries of the plastic regions at a certain elevation are computed, the stresses in the elastic regions at the same elevation may be found simply by tracing straight lines, since the equality

of stress across a boundary is postulated. Therefore, there has no significance of the stress representation in the elastic regions which they assumed in their introduction of the analytical method. And, instead of a unique solution of natural state, two solutions corresponding to the active and passive limiting states are obtained, respecting the stress distribution in the plastic regions as well as Anzo's method.

As is seen from the above description, though Glover-Cornwell have proposed a valuable approach to the progressive failure of the earth embankment, introducing a concept of "reserve strength" R expressed in Eq. (6), their deduction still lacks the theoretical rigorousness, resulting that their treatment is noting else but the simplest one which has been calculated by Anzo. This Glover-Cornwell's method is used in "Treatise on Dams", published by U. S. Department of the Interior Bureau of Reclamation, but some criticism should be remained as to the above-mentioned theoretical inaccuracies.

(3) Brahtz's method.

There is another rigorous solution of stress analysis in the earth embankment adopted in "Treatise on Dams", Brahtz's method[7] The character consists in considering the critical pore pressure p_c instead of the "reserve strength" R which has been described in the preceding Glover-Cornwell's method. It is necessary to introduce the pore pressure as a part of stresses in the stability computation of earth embankments. If we start from excluding the pore pressure among the applied forces, as Brahtz has tried, the reserve strength should be expressed as a function of allowable critical value of the pore pressure. The difference is no more than what p_c is expressed in terms of the normal stress, whereas R is the shearing stress.

Brahtz's method of stress analysis uses Mohr's criterion of failure in which the above critical pore pressure p_c is considered as follows, besides the equations of stress equilibrium of soil element :

$$\frac{(\sigma_1+\sigma_2-2p_c)\sin\varphi+2C\cos\varphi}{\sigma_1-\sigma_2}=1 \qquad \cdots\cdots(7)$$

Solving this equation for p_c, it follows :

$$p_c=\frac{\sigma_2(1+\sin\varphi)-\sigma_1(1-\sin\varphi)+2C\cos\varphi}{2\sin\varphi}, \qquad \cdots\cdots(8)$$

where the principal stresses σ_1 and σ_2 in Eqs. (7) and (8) are given in the

next equation :

$$\left.\begin{matrix}\sigma_1\\ \sigma_2\end{matrix}\right\} = \frac{1}{2}\{(\sigma_x+\sigma_y)\pm\sqrt{(\sigma_x-\sigma_y)^2+4\tau_{xy}^2}\}. \qquad \cdots\cdots\cdots\cdots(9)$$

The procedure should be to determine a set of stresses which satisfy the differential equation of stress equilibrium and the given boundary conditions, and then compute by Eq. (8) the permissible or critical pore pressures p_c, and compare these with the actual pore pressures which may exist in the soil mass. If the former are sufficiently above the latter, the structure may be considered safe. The stability problem thus becomes twofold, namely ;

1) The determination of the critical or permissible pore pressures.
2) The determination of the actual or maximum pore pressures which exist under given conditions.

For the latter ones, the author describes his own method of estimation in Part II precisely, and so Brahtz's method, in which a set of stresses to be substituted in Eq. (8) in order to obtain the critical pore pressure is determined, will be discussed in the following.

Let it be considered that the embankment forms a wedge with downstream slope tan α_1, and upstream slope tan α_2. As is shown in Fig. 2, each half of

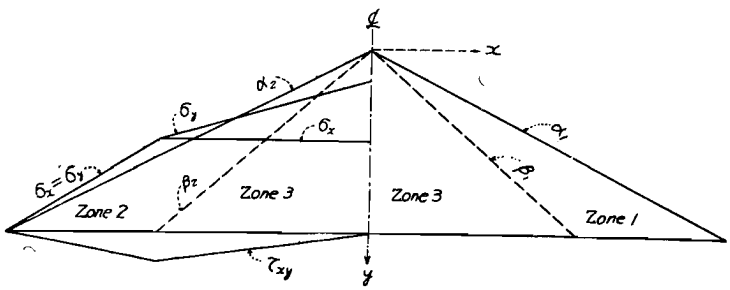

Fig. 2 Division of the embankment in Brahtz's method.

the embankment is divided into two zones by a straight line originating from the vertex of the embankment, $x=\tan\beta_1\cdot y$ or $x=\tan\beta_2\cdot y$. This angle β_1 or β_2 is one of the unknowns to be determined by the stress condition at boundaries. In each zone, the stresses are assumed to vary linearly. The unknowns in the stress equations are determined from the two equations of equilibrium and Mohr's criterion of failure. The latter is satisfied along the center line of the embankment and along the β-lines. The stress magnitudes put into Eq.

(9) are determined by assuming that the slopes of the embankment are the natural slopes of the material, and that the cohesion is equal to zero. Thus, in order to establish a critical pore pressure system at which the structure will just fail, it is often considered to be possible from the geometry of the structure and the boundary conditions, to determine a minimum value of the effective or fictitious angle of friction $\bar{\varphi}$, under which the boundary regions of structure would just be stable. With this value of $\bar{\varphi}$, a set of stresses is then determined such that the entire structure is just stable, assuming no internal pore pressures to exist. The permissible or critical pore pressures p_c are then computed by using this set of stresses in Eq. (8), but with the real physical value of the angle of friction φ as determined by field or laboratory tests. As the criterion of failure along the center line, Brahtz used the boundary condition $\sigma_x = K\sigma_y$, and he gave various values for K, as $K=0.3$, 0.5, 0.7, etc.

According to his method, the equation of β-line which divides the domain of stress in the embankment is given as follows :

$$\begin{aligned}&\tan^4\beta(\tan^2\varphi-1)-2\tan\alpha\tan^3\beta\{\tan^2\varphi(1+K)-(1-K)\}\\&+\tan^2\beta\{\tan^2\alpha\tan^2\varphi(1+K)^2-\tan^2\alpha(1-K)^2+2K(1-2K-\tan^2\varphi)\}\\&+2K\tan\alpha\tan\beta\{\tan^2\varphi(1+K)-(1-K)\}+K^2(\tan^2\varphi-1)=0. \quad\cdots\cdots\cdots(10)\end{aligned}$$

K in the above equation is the ratio of horizontal to vertical stress at the center line of the embankment, and it represents the degree of compaction of the earth embankment. As Eq. (10) is the equation of fourth order in respect of $\tan\beta$, it has two positive values for $\tan\beta$. The larger value gives the state of stress from which the critical pore pressures may be determined.

It is understood from the above description, that Brahtz's method has approached toward the unique solution of stress distribution in an earth embankment, by using the principal stress ratio K at the center of the embankment and the fictitious angle of friction $\bar{\varphi}$, in order to diminish the contradiction caused by two limiting values of the active and passive states of stress, as we have seen in the preceding discussion. His method, however, does not explain the physical meaning of β-line and the fictitious angle $\bar{\varphi}$ at all, which have been used in the deduction of his solution. As to β-line, Eq. (10) is so complicated form to compute the numerical value that the practical treatment will be of less significance. Only the introduction of the coefficient of compaction K has a unique importance, of which the precise discussion will be succeeded

as follows.

(4) Ohde's method.

An outstanding study for establishing the theory of stress distribution in the earth embankment has been performed by Ohde[8], in which the effect of fill compaction and the rigidity of embankment foundation have been accounted. In this method, in contrast with what the limiting condition for plastic equilibrium of soil constituting the embankment was used in all of the preceding methods, the stresses in the embankment at the natural state are objected from the beginning of analysis. It is considered, therefore, that the above-mentioned limiting state appears only when a particular condition of compaction and of foundation behavior is reached. An assumption is made that each of the stress components is given as the sum of two trigonometric functions approximately, in the coefficients of which is included the effect of compacting the fill material, to obtain the solution satisfying the necessary boundary conditions.

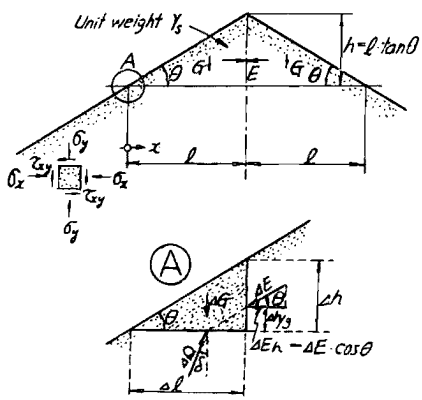

Fig. 3 Representation of the symmetrical embankment in Ohde's method.

For a symmetrical wedge-shaped embankment shown in Fig. 3, the normal stress σ_y on a horizontal section is expressed as the sum of next sine function in this method.

$$\sigma_y=\sigma_1^*\sin\left(\frac{\pi}{2}\frac{x}{l}\right)+\sigma_2^*\sin\left(\frac{3\pi}{2}\frac{x}{l}\right), \qquad \cdots\cdots\cdots\cdots(11)$$

where σ_1^*, σ_2^* are unknown functions. Using $K_1=\Delta E_h/\gamma_s\frac{(\Delta h)^2}{2}$ which is the coefficient of lateral earth pressure at the surface of slope, the following equations are deduced respecting σ_1^*, σ_2^*, from the condition for equilibrium of vertical forces in the left half of the embankment section and in the prismatic element around the point A on the surface of slope :

$$\sigma_1^*=\left\{\frac{9}{32}\pi-\frac{1}{4\pi}(1+K_1\tan^2\theta)\right\}\gamma_s h,$$

$$\sigma_2^*=\left\{\frac{3}{4\pi}(1+K_1\tan^2\theta)-\frac{3}{32}\pi\right\}\gamma_s h,$$

wherein θ is the slope angle of the embankment. On the other hand, from the condition for equilibrium of the moment of forces acting on the left half of the section about the point A, the following linear relationship exists between the coefficient of lateral earth pressure at the center of the embankment $K=E/\gamma_s \frac{h^2}{2}$ and the coefficient at the surface of slope K_1 :

$$K=\left(2-\frac{7}{\pi}+\frac{8}{\pi^3}\right)\cot^2\theta+\frac{8}{\pi^3}K_1$$
$$=0.02984\cot^2\theta+0.25801\,K_1. \qquad \cdots\cdots\cdots\cdots(12)$$

The values of these coefficients of lateral earth pressure depend on various factors such as physical properties of soil, the compaction condition of the embankment and the rigidity of the foundation. And their limiting values are provided as follows ; the minimum value of the lateral earth pressure at the center of the embankment is the active pressure ($K \geqq K_a$), and the lateral pressure at the surface of slope cannot exceed the passive earth pressure ($K_1 \leqq K_p$). According to an example that Ohde has presented for the condition of $C=0$, $\tan\varphi=0.5$ ($\varphi=26°34'$) and $\tan\theta=0.4$ ($\theta=21°48'$), one obtains $K_a=0.312$, $K_p=1.49$ by his theory of earth pressure[9], and so by Eq. (12) $K_1=0.48\sim1.49$, whose mean value is $K_1\simeq1.0$. For the embankment having a considerable rigid foundation, he has also defined the coefficient of earth pressure at rest $K_0=\sigma_x/\sigma_y$ at the center of the embankment, and has given a numerical example for the above-mentioned condition, shown in Table 1.

Table 1 Coefficient of earth pressure at rest K_0 in relation to K_1.

K_1	1.0	1.15	1.3
σ_x	0.4445	0.483	0.522
σ_y	0.810	0.802	0.795
K_0	0.549	0.602	0.658

As to the horizontal compressive stress σ_x and the shearing stress τ_{xy}, the following equations are used :

$$\sigma_x=\bar{\sigma}_1\sin\left(\frac{\pi}{2}\frac{x}{l}\right)+\bar{\sigma}_2\sin\left(\frac{3\pi}{2}\frac{x}{l}\right), \qquad \cdots\cdots\cdots\cdots(13)$$
$$\bar{\sigma}_1=\frac{1}{4}\left(\frac{2}{\pi}K_1+3K\right)\gamma_s h,$$
$$\bar{\sigma}_2=\frac{1}{4}\left(\frac{2}{\pi}K_1-K\right)\gamma_s h,$$
$$\tau_{xy}=\tau_1\sin\left(\pi\frac{x}{l}\right)+\tau_2\sin\left(2\pi\frac{x}{l}\right), \qquad \cdots\cdots\cdots\cdots(14)$$

$$\tau_1 = \frac{\pi}{4} K \tan\theta \cdot \gamma_s h,$$

$$\tau_2 = \left(\frac{K_1}{\pi} - \frac{\pi}{4} K\right) \tan\theta \cdot \gamma_s h.$$

As is clear from Eqs. (11), (12), (13) and (14), every coefficient which determines stress components depends only on the coefficient of earth pressure at the surface of slope K_1, which is the function of the compaction condition of the embankment and the rigidity of the foundation. For example, the rigid foundation has larger K_1-value than that of the flexible one, resulting larger value of stress components. Fig. 4 shows

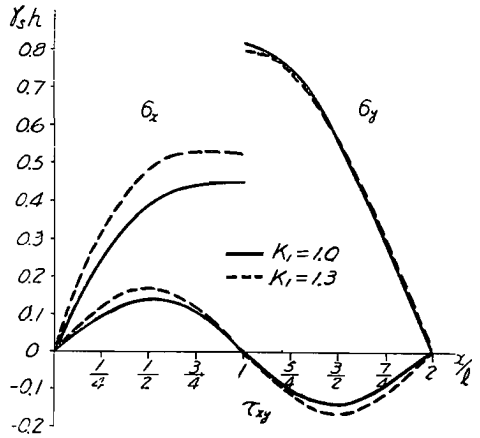

Fig. 4 Distribution of the stress components in the symmetrical embankment of 1 2.5-slope for $K_1=1.0$ and 1.3, respectively.

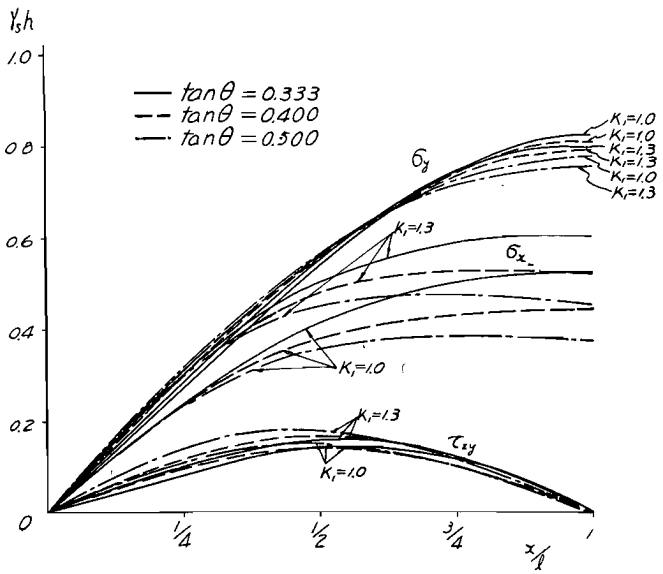

Fig. 5 Distribution of the stress components in the symmetrical embankments of various slopes for $K_1=1.0$ and 1.3, respectively.

a comparison of this character with $K_1=1.0$ and 1.3, in the case of the slope of tan $\theta=0.40$. Fig. 5 is the result of computing the stress distribution with $K_1=1.0$ and 1.3, when the slope of embankment is tan $\theta=0.50$, 0.40 and 0.333, respectively. From this figure, the distribution of the ratio σ_x/σ_y and σ_2/σ_1 on a horizontal section of embankments is obtained as shown in Fig. 6. It is seen

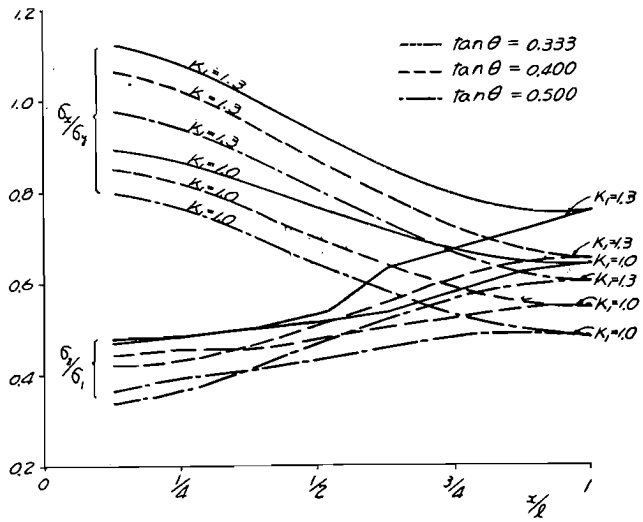

Fig. 6 Distribution of σ_x/σ_y and σ_2/σ_1 on a horizontal section of embankments.

that these ratios have larger value, if the slope of embankment is flatter and the coefficient K_1 is larger.

As is described above, in Ohde's method, the stress distribution in the embankment can be determined by the coefficient of earth pressure at the surface of slope K_1, which is designated as the degree of compaction of the fill material, being relative to the rigidity of the foundation. In this method, however, the assumption is finitely involved that each of stress components is expressed as the sum of two trigonometric functions. The affirmation should be checked by experiment.

3. Residual Strength in Author's Analytical Method

Accepting the significance of the "reserve strength" R in Eq. (6) which has been suggested by Glover-Cornwell, and in order to determine its distribu-

tion in the earth embankment, the author wishes to clear the relationship between the stress distribution in the natural state and the reserve strength by Fig. 7, excluding the mechanical division of regions as explained in the preceding article. Let it be assumed that the stresses in the earth mass in the natural state are shown by a point P in this figure. The abscissa OA of P represents the vertical compressive stress σ_y, and $\sigma_x = OB$ is the horizontal compressive stress. Conjugate shearing stresses $\tau_{xy} = PA$, $\tau_{yx} = QB$ have a same magnitude in their absolute values. If the stresses σ_x, σ_y, and $\tau_{xy} = \tau_{yx}$ at a point are under equilibrium, the ends of the vectors representing these values are located at a Mohr's circle C_0. On the other hand, the shearing resistance of soil is generally represented by a line O_1M passing through the origin O_1, from the result of the triaxial compression test. If σ_x is being reduced gradually while σ_y is unchanged, the Mohr's circle C_0 shifts to the left from the original position until it touches the straight line of rupture O_1M (circle C_A). At this condition, the earth mass is under the active state, namely under the lateral stretching ($\sigma_y > \sigma_x$). And if σ_x is being increased adversely, circle C_0 shifts to the right until it touches again the line O_1M (circle C_P). This is the passive state, and the earth mass is under the lateral compression ($\sigma_y < \sigma_x$).

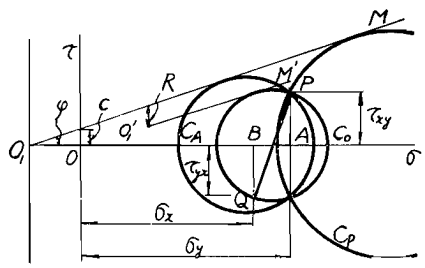

Fig. 7 Mohr's stress circles and the residual strength R.

Representing Eq. (6) using three stress components σ_x, σ_y and τ_{xy}, the following equation is obtained :

$$R = C + \tan\varphi \frac{\sigma_x + \sigma_y}{2} - \frac{1}{2\cos\varphi}\sqrt{(\sigma_x - \sigma_y)^2 + 4\tau_{xy}^2}\,. \qquad \cdots\cdots(15)$$

The author calls R in Eq. (15) the "residual shearing resistance", or the "residual strength" When the earth mass is at the limiting condition of either active or passive state above-mentioned, it can be easily understood that the mass is under the condition for plastic equilibrium, as R in Eq. (15) is equal to zero. Graphically, the "reserve strength" in Eq. (6) is the vertical distance between different points of Mohr's circle C_0 and the line O_1M, and its minimum value, that is the "residual shearing resistance" in Eq. (15), is the ver-

tical distance between parallel lines O_1M and $O_1'M'$, the latter being tangent to the circle C_0. Through this graphical explanation, it will be recognized that a rupture of the earth mass happens progressively by the encroachment on the reserve resistance R in Eq. (6) or Eq. (15), with the increase of the shearing stress by external forces acting on it.

As is described in **2. (3)**, the concept of the critical pore pressure in Brahtz's method is no more than representation of the above residual shearing resistance R in the form of the normal stress. The shearing strength of soil in which the internal pore pressure w exists is represented in the following equation, generally :

$$\tau = C + (\sigma_n - w) \tan \varphi . \qquad \cdots\cdots\cdots\cdots\cdots\cdots (16)$$

Showing this equation by Mohr's stress circle, the left circle in Fig. 8, the center of which is moved to the left equal to w from the original position, is drawn. Putting $w = p_e$ and $p_e \tan \varphi = R$ in Eq. (16), we obtain Eq. (6).

The distribution of the residual strength R in the embankment defined in Eq. (15) is shown in Table 2 and Fig. 9 for $\varphi = 26°34'$ and $C = 0$, using the

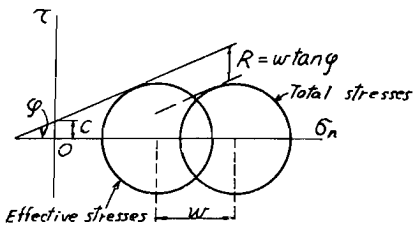

Fig. 8 Mohr's stress circles in terms of total stresses and of effective stresses.

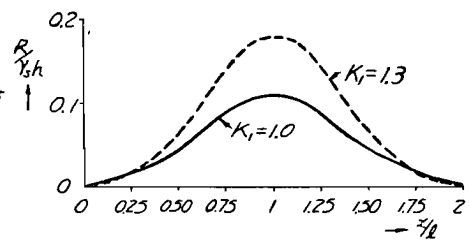

Fig. 9 Distribution of the residual strength in the embankment of 1 : 2.5-slope for $K_1 = 1.0$ and 1.3, respectively.

result of Fig. 4. As is seen by Fig. 9, a large amount of the residual strength is reserved at the central portion of the earth embankment. Comparing the case of $K_1 = 1.0$ with $K_1 = 1.3$, it is seen that the latter case has larger residual strength, and therefore, the effect of compaction is remarkable for the stability of earth embankments.

Table 2 Distribution of the residual strength R in the embankment.

x/l	0.125	0.25	0.375	0.5	0.625	0.75	0.875	1.0
$K_1 = 1.0$	0.0097	0.0216	0.0296	0.0499	0.0690	0.0892	0.1039	0.1096
$K_1 = 1.3$	0.0079	0.0181	0.0387	0.0698	0.1049	0.1408	0.1687	0.1773

4. Solution by Polar Co-Ordinate

The equation of stress equilibrium of a small soil element in the plane-strain problem is represented as follows, using the polar co-ordinate when the tensile stress is refered positive sign :

$$\left.\begin{aligned} &\frac{\partial \sigma_r}{\partial r}+\frac{1}{r}\frac{\partial \tau_{r\theta}}{\partial \theta}+\frac{\sigma_r-\sigma_\theta}{r}+\gamma_s\cos\theta=0\,,\\ &\frac{1}{r}\frac{\partial \sigma_\theta}{\partial \theta}+\frac{\partial \tau_{r\theta}}{\partial r}+\frac{2\tau_{r\theta}}{r}-\gamma_s\sin\theta=0\,, \end{aligned}\right\} \quad \cdots\cdots\cdots\cdots(17)$$

where γ_s is the unit weight of soil. If the stress components are represented in the following form using a stress function F, they satisfy Eq. (17) :

$$\left.\begin{aligned} \sigma_r&=\frac{1}{r^2}\frac{\partial^2 F}{\partial \theta^2}+\frac{1}{r}\frac{\partial F}{\partial r}-\frac{2}{3}\gamma_s r\cos\theta\,,\\ \sigma_\theta&=\frac{\partial^2 F}{\partial r^2}\,,\\ \tau_{r\theta}&=-\frac{\partial}{\partial r}\left(\frac{1}{r}\frac{\partial F}{\partial \theta}\right)+\frac{1}{3}\gamma_s r\sin\theta\,. \end{aligned}\right\} \quad \cdots\cdots\cdots\cdots(18)$$

Stresses in an embankment should satisfy the next equation at every point, according to the condition of limiting equilibrium where the residual strength γ_i^2 is considered.

$$G=\sigma_r{}^2+\sigma_\theta{}^2-2(1+2\tan^2\varphi)\,\sigma_r\sigma_\theta+4(1+\tan^2\varphi)\,\tau_{r\theta}{}^2+\gamma_i^2=0\,, \quad \cdots\cdots\cdots\cdots(19)$$

where φ is the angle of internal friction of the fill material and γ_i^2 is a variable which has positive sign in its ordinary state, although it reaches zero at the limiting state of failure.

The stress function F in Eq. (18) must be chosen so as to satisfy the above function G and boundary conditions. Assuming that f is a continuous function of θ, F is represented in the following Fourier's series :

$$\begin{aligned} F&=r^{m+2}f(\theta)\\ &=r^{m+2}\sum_{n=0}^{\infty}\{A_n\cos n\theta+B_n\sin n\theta\}\,, \end{aligned} \quad \cdots\cdots\cdots\cdots(20)$$

wherein A_n and B_n : constants, m : a number refered to the stress condition at boundaries, and n : a positive integer. Substituting Eq. (20) into Eq. (18), stress components at the arbitrary point in an embankment are given as follows :

$$\left.\begin{aligned}
\sigma_{r,n} &= r^m(m+2-n^2)\sum_{n=0}^{\infty}\{A_n\cos n\theta+B_n\sin n\theta\}-\frac{2}{3}\gamma_s r\cos\theta\,.\\
\sigma_{\theta,n} &= r^m(m+2)(m+1)\sum_{n=0}^{\infty}\{A_n\cos n\theta+B_n\sin n\theta\}\,.\\
\tau_{r\theta,n} &= r^m(m+1)n\sum_{n=0}^{\infty}\{A_n\sin n\theta-B_n\cos n\theta\}+\frac{1}{3}\gamma_s r\sin\theta\,.
\end{aligned}\right\}\qquad(21)$$

For example, when such a case is treated that a symmetrical embankment which has a triangular section of 1 : 2.5-slope is subjected to its own weight, $m=1$ and $n=1, 2, \cdots\cdots, 5$ are chosen. Then,

$$\left.\begin{aligned}
\sigma_r &= r(2A_1\cos\theta-A_2\cos 2\theta-6A_3\cos 3\theta-13A_4\cos 4\theta\\
&\qquad -22A_5\cos 5\theta-\frac{2}{3}\gamma_s\cos\theta)\,,\\
\sigma_\theta &= r(6A_1\cos\theta+6A_2\cos 2\theta+6A_3\cos 3\theta+6A_4\cos 4\theta+6A_5\cos 5\theta)\,,\\
\tau_{r\theta} &= r(2A_1\sin\theta+4A_2\sin 2\theta+6A_3\sin 3\theta+8A_4\sin 4\theta\\
&\qquad +10A_5\sin 5\theta+\frac{1}{3}\gamma_s\sin\theta).
\end{aligned}\right\}\qquad(22)$$

The boundary conditions at the slope ($\theta=68°12'$) are $\sigma_r=\sigma_\theta=\tau_{r\theta}=0$. They are put into Eq. (22) to vanish constants A_1, A_2, A_3, and new constants $A'_4=A_4/\gamma_s$ and $A'_5=A_5/\gamma_s$ are designated. Let it be assumed that $\tan\varphi=0.5$ and $\gamma_i^2\geqq 0$ in Eq. (19), we obtain

$$G=\sigma_r^2+\sigma_\theta^2-3\sigma_r\sigma_\theta+5\tau_{r\theta}^2\leqq 0. \qquad\cdots\cdots\cdots\cdots\cdots(23)$$

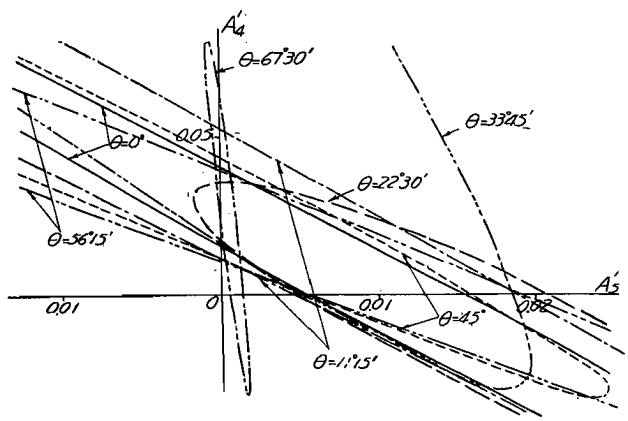

Fig. 10 Correlation between the parameters A'_4 and A'_5.

Then the above σ_r, σ_θ, $\tau_{r\theta}$ are put into Eq. (23), and $\theta=0°$, 11°15′, 22°30′, 33°45′, 45°, 56°15′ and 67°30′ are calculated to obtain domains where Eq. (23) is held. The result is shown in Fig. 10, where the inner part of every ellipse accords with this condition. As is seen from Fig. 10, we can assume that $A'_5 \simeq 0$. When this assumption is accepted, stress components at the center of the embankment are given by the following equations :

$$[\sigma_y/\gamma_s y]_{x=0}=[\sigma_r/\gamma_s r]_{\theta=0}$$
$$=-10.838A'_4+0.922,$$
$$[\sigma_x/\gamma_s y]_{x=0}=[\sigma_\theta/\gamma_s r]_{\theta=0}$$
$$=22.986A'_4+0.060.$$

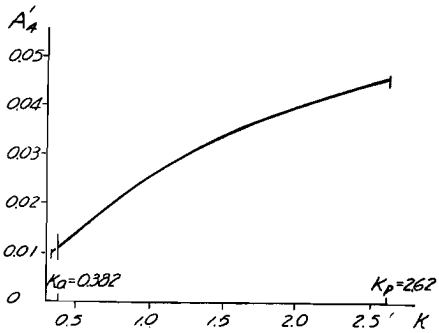

Fig. 11 Correlation between the parameter A'_4 and the coefficient K.

Assuming K is the ratio $[\sigma_x]_{x=0}/[\sigma_y]_{x=0}$, which represents the degree of compaction of the embankment, we obtain

$$\left.\begin{aligned} &K_a \leqq K \leqq K_p, \\ &\text{where } K_a=\frac{1-\sin\varphi}{1+\sin\varphi}, \\ &K_p=\frac{1+\sin\varphi}{1-\sin\varphi} \end{aligned}\right\} \quad (24)$$

The range of K is $0.382 \leqq K \leqq 2.62$, and the relationship between K and A'_4 is shown in Fig. 11. The author has calculated the stress components in the embankment from Eq. (22),

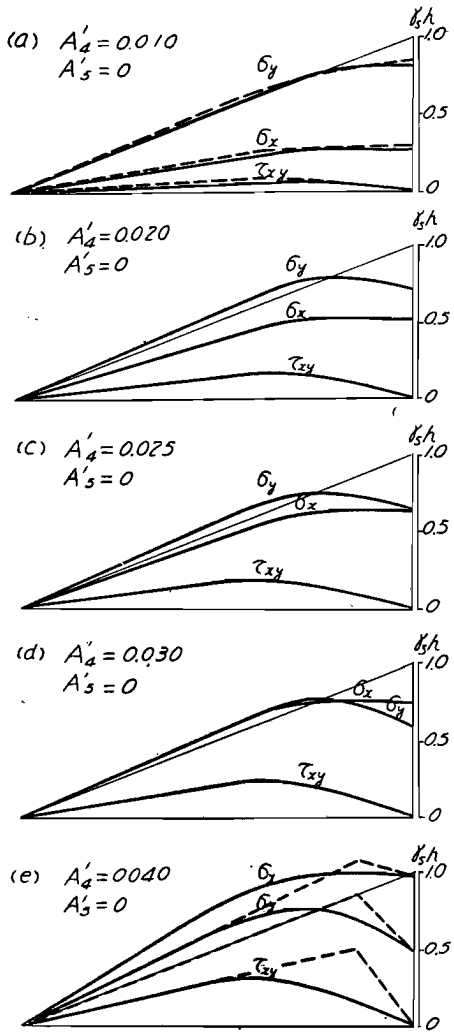

Fig. 12 Solutions of the stress distribution in the embankment of 1 : 2.5-slope by polar co-ordinate.

using values in the range of A'_4, and they have been transformed into the rectangular co-ordinate system as shown in Fig. 12. It is clear that Fig. 12 (a) is nearly equal to the active state and Fig. 12 (e) is the passive state, comparing with the solution by Anzo's method shown by the dotted lines. According to Fig. 11, the behavior of the stress distribution in the earth embankment is greatly influenced by the coefficient of compaction K. When this value is obtained experimentally, we can designate the value of A'_4 in Fig. 10 as a function of compaction.

In the analytical method described in this article, the choice of n in Eq. (21) is arbitrary, and the more number of terms of series is taken, the more precise the solution becomes. According to Jonson's investigation described in **2.** (**1**), however, it is shown that the choice of parameter in $n=4$ or 5 does not largely influence to the result.

5. Solution by Rectangular Co-Ordinate

The equation of limiting equilibrium where the residual strength R' is considered is represented in the following form, referring Fig. 13 by the rectangular co-ordinate :

$$G'=\sqrt{\left(\frac{\sigma_y-\sigma_x}{2}\right)^2+\tau_{xy}{}^2}+R'-\frac{\sigma_y+\sigma_x}{2}\sin\varphi=0. \quad \cdots\cdots\cdots\cdots(25)$$

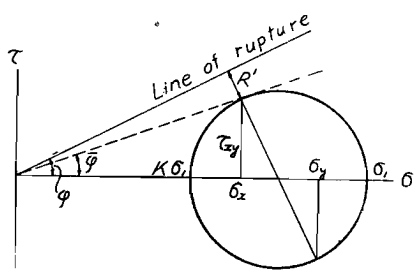

Fig. 13 Mohr's stress circle at rest and the residual strength R'

Provided σ_1 is one of the principal stresses and $K\sigma_1$ $(K>0)$ is another of them, R' in Eq. (25) is written in the next equation as shown in Fig. 13 :

$$R'=\frac{\sigma_1}{2}\left\{(1+K)\sin\varphi-(1-K)\right\}. \quad \cdots\cdots\cdots\cdots(26)$$

When $K>1$, the substitution of $K'=1/K$ in Eq. (26) is adopted. On the other hand, the relationship between the principal stress and stress components is

$$\sigma_1=\frac{\sigma_y+\sigma_x}{2}+\sqrt{\left(\frac{\sigma_y-\sigma_x}{2}\right)^2+\tau_{xy}{}^2} \quad \cdots\cdots\cdots\cdots(27)$$

Putting Eq. (27) into Eq. (25), the following equation is obtained.

$$\left.\begin{aligned} &G=(\sigma_y-\sigma_x)^2+4\tau_{xy}{}^2-A^2(\sigma_y+\sigma_x)^2=0\,, \\ &\text{where}\qquad A=\frac{1-K}{1+K}=\sin\bar{\varphi} \end{aligned}\right\} \qquad \cdots\cdots\cdots\cdots(28)$$

The equation of limiting equilibrium with the residual strength is, therefore, represented in a very simple form as Eq. (28), using the virtual angle of resistance $\bar{\varphi}$ instead of the angle of internal friction $\bar{\varphi}$ at failure. The virtual angle of resistance is the friction angle corresponding to the mobilized part of the internal friction of the fill material[10], and it has not a unique value for whole embankment but varies with the location by the author's analysis. K in Eq. (26) and Eq. (28) is the coefficient of lateral earth pressure or the coefficient of earth pressure at rest, as is already shown in the preceding article, which is a function of the degree of compaction of the embankment, and it exists between next two limiting values.

$$\left.\begin{aligned} &\frac{1}{N_\varphi}\leqq K\leqq N_\varphi\,, \\ &\text{where}\qquad N_\varphi=\tan^2\left(45^\circ+\frac{\varphi}{2}\right). \end{aligned}\right\} \qquad \cdots\cdots\cdots\cdots(29)$$

In the author's method, the assumption that stress components may be expressed by the linear function of x and y in each of elementary wedges as the same as Anzo's method is accepted. Then, at the adjacent part of slope :

$$\left.\begin{aligned} &[\sigma_y]_s=\gamma_s[A_s x+(B_s-1)y]=-\gamma_s(x\tan\theta-y)(D_s\tan^2\theta-1)\,, \\ &[\tau_{xy}]_s=-\gamma_s[B_s x+C_s y]=-\gamma_s(x\tan\theta-y)D_s\tan\theta, \\ &[\sigma_x]_s=\gamma_s[C_s x+D_s y]=-\gamma_s(x\tan\theta-y)D_s\,. \end{aligned}\right\} \qquad \cdots\cdots(30)$$

The physical meaning of coefficients A_s, B_s, C_s, D_s is cleared by Fig. 14, and when the coefficient of lateral earth pressure at the slope D_s is assumed, the others are determined dependently. In Anzo's method, as the value corresponding to the limiting state,

$$D_{R,\substack{max\\min}}=-\cos^2\theta\frac{\cos\theta\mp\sqrt{\cos^2\theta-\cos^2\varphi}}{\cos\theta\pm\sqrt{\cos^2\theta-\cos^2\varphi}} \qquad \cdots\cdots\cdots\cdots(31)$$

is treated. In the author's method, however, the coefficient D_s from Eq. (29) :

$$D_{R'min}\leqq D_s\leqq D_{R'max} \qquad \cdots\cdots\cdots\cdots(32)$$

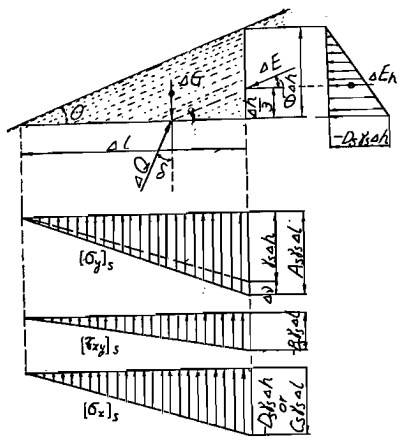

Fig. 14 Distribution of the stress components in the adjacent part of slope.

is adopted instead of D_R. The value of D_s has a close relationship with the degree of compaction of the earth embankment ; the greater the effect of compaction is, the larger the absolute value of D_s becomes. This relation is found definitely through a simple model experiment described in the following article.

Determining the coefficients of earth pressure near the slope of the embankment, then the condition of stress continuity and of limiting equilibrium with residual strength can be used on the boundaries of arbitrarily divided wedges, just similarly to Anzo's method ; i. e. at $x/y=\tan\alpha_i$:

$$\left.\begin{aligned}&[\sigma_y]_i=[\sigma_y]_{i+1},\quad [\tau_{xy}]_i=[\tau_{xy}]_{i+1},\quad [\sigma_x]_i=[\sigma_x]_{i+1},\\&\{[\sigma_y]_i-[\sigma_x]_i\}^2+4[\tau_{xy}]_i^2-\sin^2\bar{\varphi}_i\{[\sigma_y]_i+[\sigma_x]_i\}^2=0\,.\end{aligned}\right\}\quad\cdots\cdots\cdots\cdots(33)$$

The virtual angle of resistance $\bar{\varphi}_i$ in Eq. (33) is determined experimentally from Eq. (28), as a function of compaction of the earth embankment, and $\bar{\varphi}_i<\varphi$ so long as the embankment is under stable at rest. By solving these equations simultaneously, the coefficients of earth pressure A_i, B_i, C_i, D_i which are proper for each divided wedges are obtained. Three or four divisions of domain are adequate for a half of embankment.

Let it be taken as a calculating example that has been presented in the preceding article ; the stress distribution in a symmetrical embankment with a triangular section of 1 : 2.5-slope subjected to its own weight only. As is shown in Fig. 15, a half of the symmetrical embankment is divided into three wedges, and suffixes I, II and S are given for them, respectively. Taking $\tan\varphi=0.5$ again, from Eq. (31) and Eq. (32),

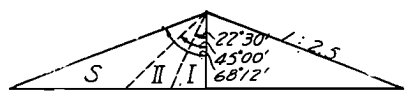

Fig. 15 Division of embankment into small wedges.

$$-0.4975\geq D_s\geq -1.493\,,$$

Therefore, $D_s=-1.0$ can be taken. In this case, $A_s=0.464$, $B_s=-0.16$ and $C_s=0.4$. The ratio of increment of σ_x to σ_y at the slope region is

$$K_s=\frac{\partial[\sigma_x]_s}{\partial x}\Big/\frac{\partial[\sigma_y]_s}{\partial x}=\frac{\gamma_s C_s}{\gamma_s A_s}=0.862\,.$$

Therefore, $D_s=-1.0$ corresponds to the coefficient of earth pressure in the case of the ratio $K_s=0.862$. For the embankment which is compacted as greater as $K_s=1.0$, the coefficient is $D_s=-1.19$. The approximate value of this ratio K_s is known by the simple experiment described later. The coefficient of earth pressure at rest K at the center of the embankment can be also taken as $K=0.8$ experimentally. Then, A in Eq. (28) becomes $A=\sin\bar{\varphi}=0.111$. In this example, thus designated, Eq. (33) results in the following equations.

$$\left.\begin{array}{ll}
\text{a) at } x/y=0: & \\
\quad [\tau_{xy}]_I=0 & C_I=0, \\
\quad G=0 & (B_I-1-D_I)^2+4C_I^2-0.0123(B_I-1+D_I)^2=0, \\
\text{b) at } x/y=0.4142: & \\
\quad [\sigma_y]_I=[\sigma_y]_{II} & 0.4142(A_I-A_{II})+(B_I-B_{II})=0, \\
\quad [\tau_{xy}]_I=[\tau_{xy}]_{II} & 0.4142(B_I-B_{II})+(C_I-C_{II})=0, \\
\quad [\sigma_x]_I=[\sigma_x]_{II} & 0.4142(C_I-C_{II})+(D_I-D_{II})=0, \\
\text{c) at } x/y=1.0: & \\
\quad [\sigma_y]_{II}=[\sigma_y]_s & (A_{II}-0.464)+(B_{II}+0.16)=0, \\
\quad [\tau_{xy}]_{II}=[\tau_{xy}]_s & (B_{II}+0.16)+(C_{II}-0.4)=0, \\
\quad [\sigma_x]_{II}=[\sigma_x]_s & (C_{II}-0.4)+(D_{II}+1.0)=0.
\end{array}\right\}\quad\cdots(34)$$

As there exist eight equations in Eq. (34) for eight unknowns A_I, B_I, C_I, D_I, A_{II}, B_{II}, C_{II} and D_{II}, it is possible to solve the simultaneous equation. Solving these equations, the representation of the stress distribution for

Table 3 Stress distribution for each divided region in the embankment.

	Ist-region $0<x/y<0.4142$	IInd-region $0.4142<x/y<1.0$	S-region $1.0<x/y<2.5$
σ_y/γ_s	$0.0413x-0.7532y$	$0.0687x-0.7637y$	$0.464x-1.16y$
$-\tau_{xy}/\gamma_s$	$0.2468x$	$0.2363x+0.0047y$	$-0.16x+0.4y$
σ_x/γ_s	$-0.6027y$	$0.0047x-0.6047y$	$0.4x-1.0y$

each wedge-shaped domain in the embankment is shown in Table 3.

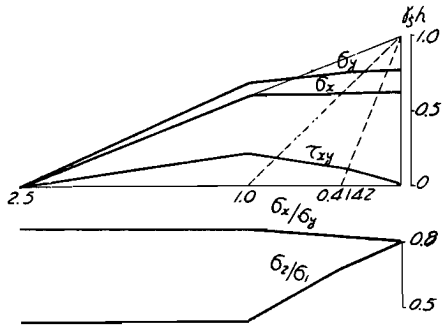

Fig. 16 Solution of the stress distribution in the embankment of 1 2.5-slope by rectangular co-ordinate.

The result of numerical calculation is given in Fig. 16, which is similar to Fig. 12(c) described in the preceding article. The distribution of the normal stress ratio σ_x/σ_y and the principal stress ratio σ_2/σ_1 is also shown in Fig. 16. It is clear that the assumption used in the calculation are fully satisfied and that the behavior of the distribution of stress components can be accepted reasonably.

6. Experiment by Sand Models

The author has performed some experimental investigation using sand

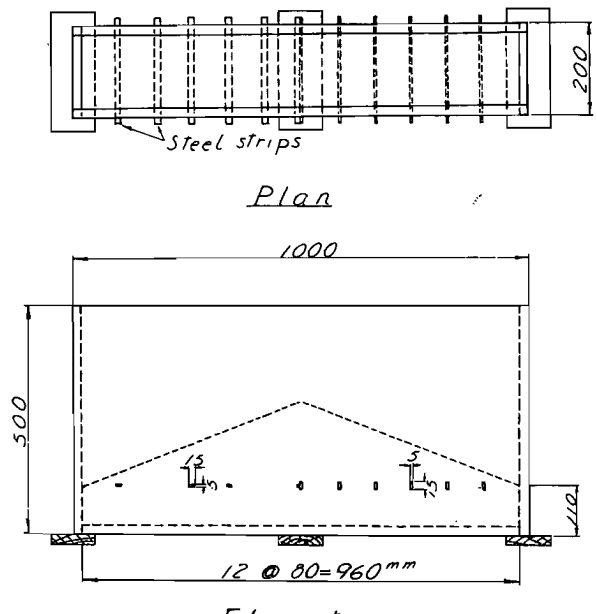

Fig. 17 Experimental apparatus.

models, in order to know the stress distribution in the earth embankment, and to ascertain the above-mentioned theories. In these models, measurements of the vertical compressive stress σ_y and the horizontal stress σ_x are performed by using thin strips of steel installed at the place as shown in Fig. 17. A row of strips is placed horizontally for measuring σ_y, and the other is placed vertically for σ_x. After making up the model the steel strips are pulled out, and the forces required to make them move are measured. The air-dried uniform sand of which the average diameter is about 0.2 mm is used for the embankment material, and the slope and the degree of compaction is varied in three kinds, respectively.

For example, Fig. 18 shows the result of test in the case of 1 : 2.5-slope, stresses being given in terms of $\sigma_y/\gamma_s h$ and $\sigma_x/\gamma_s h$, respectively, wherein h is the height of the model embankment.

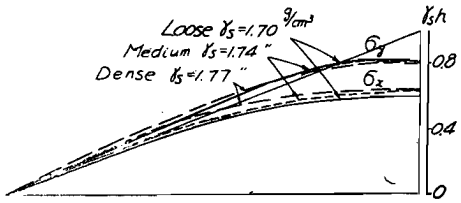

Fig. 18 Stress distribution in the embankment of 1 : 2.5-slope in terms of compactness.

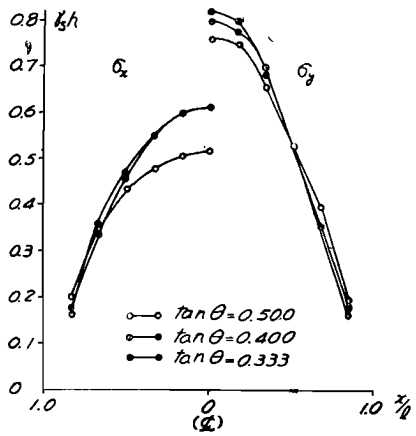

Fig. 19 Stress distribution in the embankment of medium compaction in terms of slope.

Fig. 19 is the stress distribution for the medium compaction ($\gamma_s = 1.73 \sim 1.74$ g/cm³), when the abscissa is given in the form of x/l. According to this figure, although σ_y does not vary so largely with the slope of the embankment, σ_x varies in a wide range. It is easily seen from Fig. 18 that as the degree of compaction increases σ_x becomes larger for the embankment of the same slope, whereas σ_y does not vary so remarkably. The ratio σ_x/σ_y on a horizontal section in the embankment is large when the slope is flatter, as shown in Fig. 20. The coefficient of compaction K at the center of the embankment is in the range of 0.6~0.85. Provided that the rigidity of foundation is small, K will decrease to its lowest value of the active pressure.

In any circumstances, if we know the approximate value of the coefficient

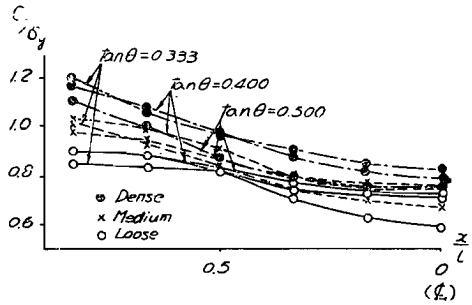

Fig. 20 Distribution of the ratio of σ_x/σ_y in the embankments of various slopes and compactnesses.

of compaction K experimentally, for the various states of embankment material, the stress distribution can be calculated easily by the theoretical equations which have been deduced by the author.

7. Conclusion

Although the Swedish slip circle method in the stability analysis of earth embankments is so practical in the application that the disadvantage of very tedious iteration of the trial calculation might be partly covered, the degree of safety against the progressive failure cannot be estimated quantitatively. The author has stood on the more analytical view-point and studied of the relation between the stress distribution and the degree of compaction of the earth embankment, theoretically and experimentally. In the theoretical stress analysis, the equation of limiting equilibrium with the residual strength has been used, in order to be free from the inconsistency involved in conventional studies. Then, the reasonability of the author's analysis has been ascertained throughout the model experiment.

Examples of the theoretical analysis and the model experiment illustrated in this paper are the results for very simple case of stress conditions, for the sake of facilitating the understanding. However, they can be applied broadly to more complex problems.

Part II Effect of the Pore Pressure on the Stability of Earth Embankments

1. Introduction

The stability analyses of an earth embankment with respect to the pore pressure consist of the following items ;

1) Stability analyses of the dam and the foundation, respectively, during construction (due to the non-steady pore pressure).
2) Stabitity analysis of the dam for rapid-drawdown of the reservoir (due to the transient pore pressure).
3) Stability analyses of the dam and the foundation, respectively, for full reservoir (due to the steady seepage pressure).

For the last item, the analyses can be easily performed by drawing a flow-net for the steady stream flow, and finding the statical head at each point in the figure. The author has pointed out, through the experimental studies of percolating flow using sand models, that the local failure near the upper portion of the surface of seepage is predominant, in the case of the water-retaining embankment which consists of cohesionless materials. In these studies, performing the theoretical investigations concerning these experimental results, a proposed equation which gives the critical hydraulic gradient has been deduced for this kind of local failure, whereby the mechanism of the actual failure of embankments can be analysed[11] Further experimental research has been succeeded towards the disaster preventive methods of embankment design, and a reasonable criterion has been given adequately[12]

Among the first item, the author has made a theoretical study for the stability analysis of the dam foundation during and just after construction, in connection with the execution control of fill work[13] In this study, starting from the fundamental theoretical equation of the two-dimensional consolidation, the distribution of the pore pressure in the embankment foundation has been studied theoretically. Next, by using the above solutions, the plasticity load in the foundation where the pore pressure exists has been obtained throughout the numerical calculation.

Thus the remaining problems, the pore pressure coming into existence in

the earth embankment due to the consolidation of the fill material during construction, and the residual pore pressure after rapid-drawdown of the reservoir, are treated as the second part of this paper.

2. Distribution of Pore Pressure during or Just after Construction

(1) General consideration.

In the embankment composed of relatively impervious materials as the earth dam, the pore pressure occurs in itself due to the consolidation of soil during construction[14]. It seems somewhat difficult to estimate the distribution of the pore pressure theoretically, comparing with that of the embankment foundation which has been tried in the preceding paper. The reason is, that the geometry of the surface of earth fill where the boundary conditions should be given varies with the construction process, and that it is not easy to obtain the solution of two-dimensional consolidation, even if the shape of embankment is very simple. As in some conventional studies for estimating the pore pressure during construction of the earth embankment, bold assumptions have been used to simplify the complicated problem, these theoretical solutions are not always satisfactory when compared with the measured data observed in the field[15][16]

In the author's method, the consolidation process is treated as a heaping phenomenon by the sedimentation of unsaturated soils, and he applies the approximate solution using a parabolic pressure curve, which has been proposed by Terzaghi-Fröhlich[17] for the mechanism of consolidation of a clay layer whose thickness varies with time. Though more rigorous solution has been deduced for the mechanism of consolidation of a clay layer[18], it is not necessary to be so rigorous as this in practice.

In the solution which has been proposed by Terzaghi-Fröhlich for the consolidation of sedimentary clay layer, the following fundamental assumptions are involved :

1) one-dimensional consolidation only upwards vertically is treated,
2) coefficient of consolidation $c = k/\gamma_w m_v$ is constant during the sedimentary period,
3) velocity of sedimentation is constant,

4) pores of clay layer are fully saturated, as the sedimentation in water is considered, and

5) excess pore pressure curve is assumed as a parabola approximately.

Because of these assumptions, it is not possible to apply the above solution directly to the consolidation of earth fill during construction without some modifications. Assumptions 2), 3) and 5) are satisfied in this case, whereas it is clear that the first assumption of one-dimensional consolidation and the fourth of fully saturation are not established in the construction of embankment. In the author's method, therefore, to modify these assumptions, he considers the compressibility of containing air in the soil mass due to the unsaturation and the effect of compacting action represented by the coefficient of earth pressure at rest due to the unisotropy of stresses in the earth fill, during one-dimensional consolidation until the completion of filling. For the behavior of dissipation of the pore pressure after the completion of embankment, it is possible to compute the distribution of the pore pressure in the embankment by the approximate step-by-step method, transforming the fundamental equation of the two-dimensional consolidation into the finite differential equation.

(2) Application of Terzaghi-Fröhlich's theory.

Applying the approximate solution using a parabolic pressure curve, which has been proposed by Terzaghi-Fröhlich, to a clay layer having the initial trigonometric excess pressure, whose apex is on the upper permeable boundary, the following solutions are obtained, referring Fig. 1.

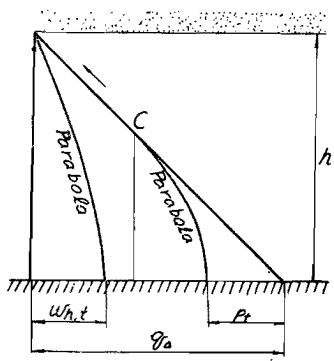

Fig. 1 Parabolic pore pressure curve to a clay layer of initial trigonometric excess pressure in Terzaghi-Fröhlich's theory.

$$\left.\begin{aligned} &1)\quad 0\leqq t\leqq \frac{1}{6}\frac{h^2}{c},\qquad 0\leqq y\leqq (h-\sqrt{6ct}):\\ &\qquad w(y,\ t)=\frac{y}{h}q_a,\\ &2)\quad 0\leqq t\leqq \frac{1}{6}\frac{h^2}{c},\qquad (h-\sqrt{6ct})\leqq y\leqq h: \end{aligned}\right\}\quad\cdots\cdots\cdots\cdots(1)$$

$$w(y,\ t)=q_{\Delta}\left\{1-\frac{1}{h}\sqrt{\frac{3ct}{2}}\left\{1+\frac{(h-y)^2}{6ct}\right\}\right\},$$

3) $\dfrac{1}{6}\dfrac{h^2}{c}\leqq t\leqq\infty,\quad 0\leqq y\leqq h$:

$$w(y,\ t)=\frac{q_{\Delta}}{2}\left\{1-\frac{(h-y)^2}{h^2}\right\}\exp\left\{-\left(\frac{3ct}{h^2}-\frac{1}{2}\right)\right\}.$$

In the consolidation of sedimentary clay layer, the initial distribution of pore pressure can be regarded as a triangle, whereby the above-mentioned solution is applicable. The depth of layer h is, however, not constant but increases with time, being represented as h_t. On the other hand, the tangential point C on the pressure curve in Fig. 1 rises upwards with time, and the vertical component of its velocity is

$$v_c=\frac{dh_c}{dt}=\sqrt{\frac{3c}{2t}}, \qquad \cdots\cdots(2)$$

and the constant velocity of sedimentation is

$$v_s=\frac{dh_t}{dt}=\text{const.} \qquad \cdots\cdots(3)$$

The difference of these two values divides the mechanism of consolidation. As is seen from Eq. (2), the velocity of consolidation v_c is independent of the thickness of clay layer ; v_c is infinite when $t=0$, and decreases with time. From Eq. (1) it can be seen that Eq. (2) holds only when $0\leqq t\leqq\frac{1}{6}\frac{h^2_t}{c}$. So the minimum v_c is

$$v_{c,min}=\frac{3c}{h_t}. \qquad \cdots\cdots(4)$$

From the above consideration, it is concluded that, when $v_s>v_{c,min}$ there is no effect of increasing thickness of layer on the consolidation. In other words the conclusion is that, there is a definite relation between the velocity of sedimentation v_s [cm/sec] and the coefficient of consolidation c [cm²/sec], where in $v_s>3c/h_t$, the increase of thickness of the layer has no effect on the consolidation, and in the initial state of $v_s<3c/h_t$, the both interact each other. Investigating this relationship between sedimentation and consolidation, Terzaghi-Fröhlich have shown, from the character of the parabolic pressure curve, that the time t_2 after which the mutual interference diminishes is :

$$t_2=1.41\,t_1=1.41\frac{3c}{v_s^2} \qquad \cdots\cdots(5)$$

The author draws Fig. 2 to facilitate our understanding of the above-mentioned relationship. The figure illustrates the relation between time : t, height of sedimentation : h_t, height of point C : h_c, velocity of sedimentation : v_s, velocity of consolidation : v_c, $v_{c,min}$, and intergranular pressure : p_t. As described above, at the initial state of sedimentation, as the velocity of consolidation v_c is greater than that of sedimentation v_s, the both interfere with each other till t_2 which is given in Eq. (5), and only in the case of $t \geqq t_2$, the increase of the depth of layer has no effect on the consolidation of soils. Consequently, in order to make the computation of consolidation more precisely, it is necessary to make the modification to the time factor as large as $\Delta t = 0.41\, t_1$.

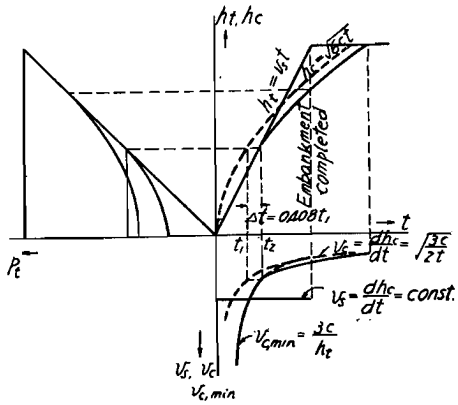

Fig. 2 Correlation between several variables during and just after construction of embankment.

(3) Pore pressure during construction.

Neverthless, it seems to be of little use to apply this consideration to the consolidation of fill material of the actual embankment. The reason is that, in the construction of the earth embankment, as the speed of filling v_s is pretty large, compared with the coefficient of consolidation c, in contrary to the geological sedimentation of earth ground, the time t_2 given by Eq. (5) is very small, accordingly the modification of the time factor is still small in practice. For example, on Fresno Dam (in U.S.A.) to which the author tries numerical calculation, whose height $h_f = 15$ m, construction period $t_f = 3$ months, speed of filling $v_s = 15\text{m}/3\text{ months} = 1.93 \times 10^{-4}$ cm/sec, and coefficient of consolidation $c = 1 \times 10^{-3}$ cm^2/sec (assuming this value from the dam material of clay gravel), we obtain from Eq. (5) $t_2 = 1.14 \times 10^5$ sec $= 31.6$ hr, being very small compared with the whole construction period of $t_f = 3$ months, and $\Delta t = 0.41\, t_1 = 3.30 \times 10^4$ sec $= 9.16$ hr only.

Fig. 3 (a) shows the result of calculating the distribution of pore pressure in Fresno Dam just after completion of 3 months' construction, under the

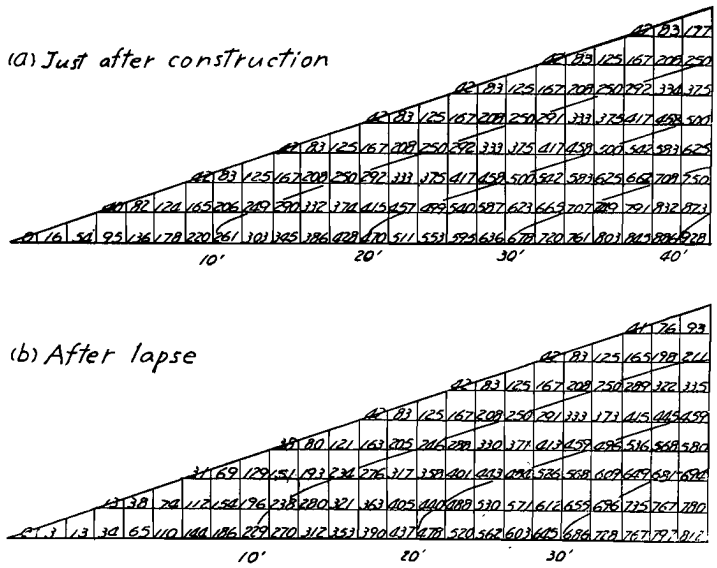

Fig. 3 Distribution of pore pressure in the embankment of 1 : 3-slope ; (a) just after 3-months' construction and (b) after 1-year from completion.

above-mentioned consideration. At the calculation, the left half of the symmetrical dam is divided into 24×8 lattices, and the pore pressure at every nodal point just after dam construction is obtained, using Eq. (1) to each vertical column thus divided. Values marked beside each nodal point represent the pore pressure, using the dam height as the measuring unit. In this figure the time factor is

$$T_v = \frac{c(t_f - \Delta t)}{h^2} = \frac{c(t_f - 0.41\,t_1)}{h^2} = 3.44 \times 10^{-3}.$$

Provided that the overall pore pressure coefficient $\bar{B}$, which has been introduced by Skempton-Bishop, i. e.

$$\frac{\Delta w}{\Delta \sigma_1} = \bar{B} = B\left\{1 - (1-A)\left(1 - \frac{\Delta \sigma_3}{\Delta \sigma_1}\right)\right\} \qquad \cdots\cdots\cdots\cdots\cdots\cdots (6)$$

is adopted $\bar{B} \simeq 0.6$ for clay gravel, considering the unsaturation of fill material and the unisotropy of stresses in the embankment as explained later, and assuming the unit weight of fill material $\gamma_s = 1.7\ \mathrm{g/cm^3}$, equi-pressure lines in Fig. 3(a) are shown in piezometric height, whereas the measured data in the field

are given in Fig. 4(a).

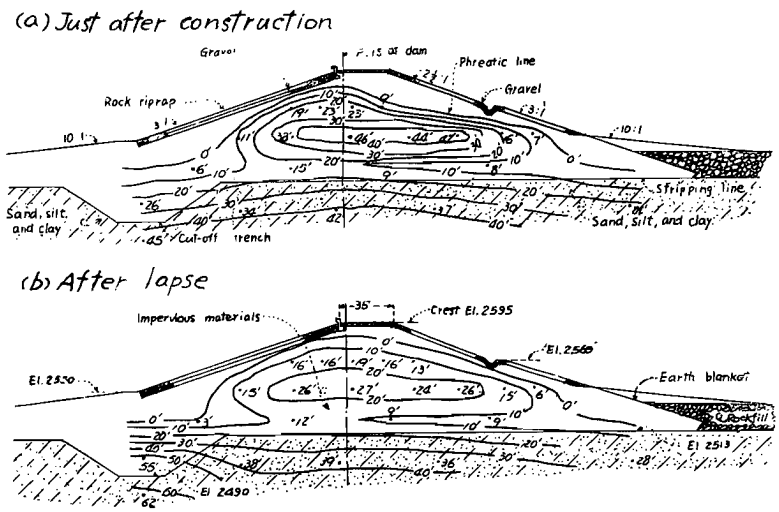

Fig. 4 Measured data of the distribution of pore pressure in Fresno Dam due to construction ; (a) just after 3-months' construction and (b) after 1-year from completion.

(4) Pore pressure after construction.

When the distribution of pore pressure in the embankment just after completion has obtained as above, then the behavior of dissipation of the pore pressure is known as follows ; the fundamental differential equation of two-dimensional consolidation

$$\frac{\partial w}{\partial t} = c\left(\frac{\partial^2 w}{\partial x^2} + \frac{\partial^2 w}{\partial y^2}\right) \qquad \cdots\cdots\cdots\cdots\cdots\cdots(7)$$

is transformed into the following finite differential equation :

$$\left.\begin{aligned} & w_0(\mathrm{t}+\delta t) = \beta(w_1+w_2+w_3+w_4-4w_0)+w_0(t)\,, \\ & \text{where} \qquad \beta = \frac{c\cdot\delta t}{(\delta h)^2}, \qquad \delta x = \delta y = \delta h \end{aligned}\right\} \quad \cdots\cdots\cdots(8)$$

The smaller the distance between nodal points of lattices δh and also the time interval δt are taken, the more precise the solution of this equation becomes[19]

To know the distribution of residual pore pressure in Fresno Dam after one year from completion (i. e. after fifteen months from starting of the construction), the numerical calculation is performed. Using $\delta h = h_f/8 = 187.5$ cm,

$\delta t = 1$ month $= 2.59 \times 10^6$sec, i. e. $\beta = c \cdot \delta t / (\delta h)^2 = 0.0737$, the approximate step-by-step method of twelve reiteration has been succeeded for all 108 nodal points. The result is given in Fig. 3(b) and the observation in the field is shown in Fig. 4(b). Comparing with each figure, owing to the existence of some permeable stratum adjacent to the dam base in the latter, the dissipation of pore pressure is sooner than the former.

As is seen by Fig. 3 and Fig. 4, the high pore pressure remains in the embankment just after completion or for a considerable period after that. The author has tried a theoretical study on the execution control of fill work on a soft foundation, as summarized in **1.**, but it is also necessary to study the same consideration even when the fill material consolidates itself. Though the above Fresno Dam was finished in three months actually, if the construction would last over one year slowly, the distribution of pore pressure is shown in Fig. 5 (a) for just after completion and in Fig. 5(b) for three months after (i. e.

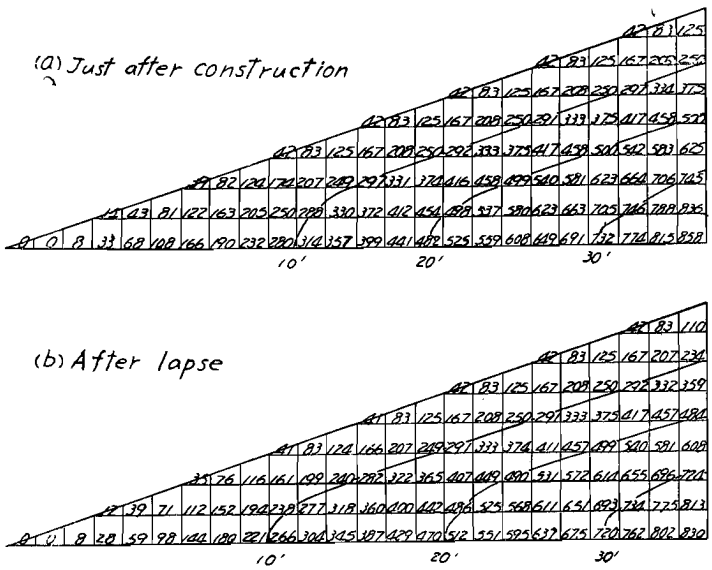

Fig. 5 Distribution of pore pressure in the embankment of 1 : 3-slope ; (a) just after 1-year's construction and (b) after 3-months from completion.

after fifteen months from starting of the construction), in which the pore pressure is pretty small except in the central part of the embankment. In this virtual case, the speed of filling is $v_s = 15$ m/1 year $= 4.74 \times 10^{-5}$ cm/sec, and the

time factor at the completion is $T_v=1.36\times10^{-2}$. At the calculation of Fig. 5 (b), $\beta=0.0737$ is used as the same as in Fig. 3(b).

As is described in the preceding part of this paper, the large amount of residual strength is reserved in the central part of the wedge-shaped embankment. As in the slope regions, however, the reserve is very small, in the case of slow dissipation of pore pressure due to the high speed of filling, it is necessary that the execution speed is lowered to decrease the pore pressure, as is shown in the above numerical calculations.

(5) Determination of pore pressure coefficient.

Pore pressures coming into existence during construction under consideration and after rapid-drawdown of the reservoir described later, occur by the change of the principal stresses in the earth embankment. Skempton[20] has given next representation of this relationship.

$$\Delta w=B[\Delta\sigma_3+A(\Delta\sigma_1-\Delta\sigma_3)], \qquad \cdots\cdots\cdots\cdots\cdots(9)$$

wherein A, B are the pore pressure coefficients. As is shown in Fig. 6, the

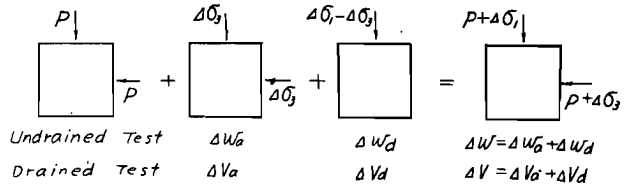

Fig. 6 Pore pressures in the triaxial test.

change of pore pressure Δw can be considered as the sum of the pore pressures by the change of ambient stress $\Delta\sigma_3$ and of deviator stress $(\Delta\sigma_1-\Delta\sigma_3)$. Thus Eq. (9) is :

$$\Delta w=\Delta w_a+\Delta w_d, \qquad \cdots\cdots\cdots\cdots\cdots(10)$$

and the pore pressure coefficients are :

$$\left.\begin{aligned} B&=\frac{\Delta w_a}{\Delta\sigma_3},\\ A\cdot B&=\frac{\Delta w_d}{\Delta\sigma_1-\Delta\sigma_3}\end{aligned}\right\} \qquad \cdots\cdots\cdots\cdots\cdots(11)$$

In computing the pore pressure during the fill construction or after rapid-drawdown of the reservoir, Eq. (9) is conveniently transformed into Eq. (6) by Bishop[21] $\bar{B}$ in this equation is called the overall pore pressure coefficient.

Generally the coefficient A is smaller than unity and in many cases is nearly equal to zero. As $\Delta\sigma_3 < \Delta\sigma_1$ in the earth embankment under construction, the overall coefficient $\bar{B}$ is smaller than the coefficient B.

The author has measured the overall pore pressure coefficient $\bar{B}$, using the triaxial compression apparatus for three kinds of soil ; coarse sand, silty sand and disturbed clay. In the measurement, the applied stress has been increased in two stages so as to use Eq. (9). The procedure is that, as is shown in Fig. 6, in the first stage, the specimen is consolidated under the all-round effective pressure p and then the change of the pore pressure Δw_a accompanied with the application of the change of the ambient pressure $\Delta\sigma_3$ under the undrained condition is measured. In the second stage, the change of deviator stress $(\Delta\sigma_1 - \Delta\sigma_3)$ is given to the specimen, and the corresponding change of the pore pressure Δw_a is measured. The measurement of the pore pressure has been performed by the porous pilot installed in the middle height of the specimen, which has been led to the manometer of no-flow type. The result is tabulated in Table 1.

Table 1 Pore pressure coefficient measured by triaxial tests.

	p(kg/cm^2)	$\Delta\sigma_3$(kg/cm^2)	Δw_a(kg/cm^2)	B	$\Delta\sigma_1$(kg/cm^2)	Δw_a(kg/cm^2)	$\bar{B}$
Coarse sand	2.0	0.2	0.10	0.50	0.50	0.08	0.36
Silty sand	2.0	0.2	0.03	0.15	0.40	0.02	0.125
Clay (disturbed)	2.0	0.5	0.45	0.90	0.95	0.20	0.68

The overall pore pressure coefficient $\bar{B}$ is much larger in clay than in sandy soil. For the clay, $\bar{B}=0.68$ has been obtained in the remolded state. This specimen is the pure clay from Ōsaka alluvial stratum. As the fill material in the actual embankment is considered to have greater permeability, $\bar{B}=0.6$ has been adopted in the preceding numerical calculations.

(6) Stability computation.

The author has performed the stability computation for an earth embankment just after construction, which has a symmetrical section of 1 : 3-slope, shown in Fig. 3. Fig. 7(a) shows the distribution of pore pressure in the embankment, which is drawn from Fig. 3(a), taking the overall pore pressure coefficient $\bar{B}=0,6$ as is described above. Assuming the mechanical properties

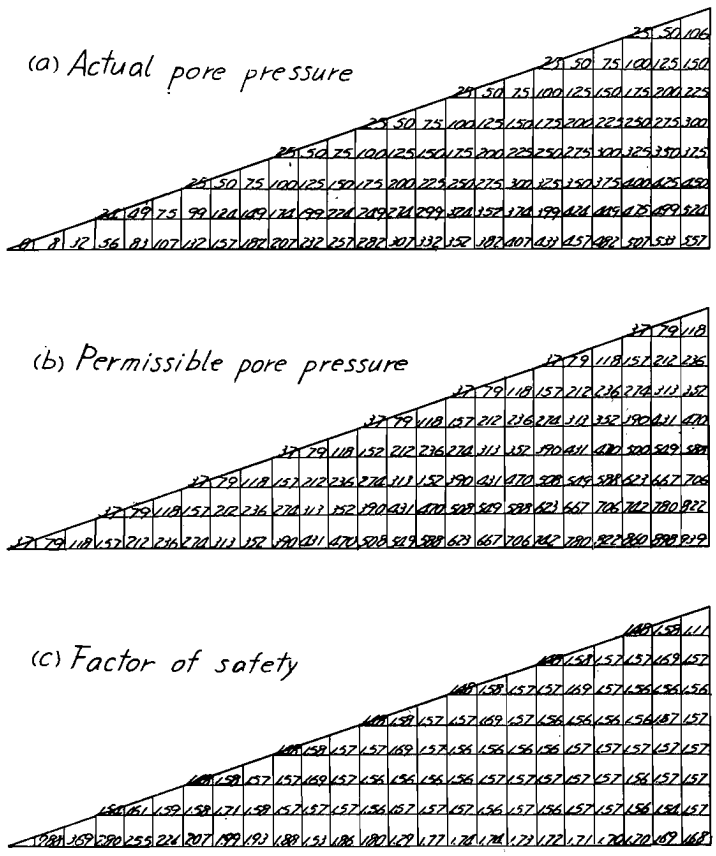

Fig. 7 Distribution of (a) actual pore pressure, (b) permissible pore pressure and (c) factor of safety in the embankment of 1 · 3-slope just after construction.

of the fill material as $K_1=1.0$, $\tan\varphi=0.5$ ($\varphi=26°34'$) and $C=0$, the permissible or critical pore pressure is shown in Fig. 7(b), calculating from the residual shearing resistance explained in the preceding part of this paper. The ratio of the permissible pore pressure (Fig. 7(b)) to the actual pore pressure (Fig. 7(a)) gives a factor of safety of the embankment just after construction, with respect to the failure due to pore pressure. Fig. 7(c) shows this value, where it is known that, in spite of the great magnitude of residual strength in the central part of the embankment, the factor of safety is small in this part, because the pore pressure occuring during construction has a considerable value.

In this calculating example, in order to compare with the measured data on Fresno Dam, the construction period is assumed three months for which Fig. 3(a) is applicable. But the larger period of construction gives higher factor of safety than that of Fig. 7(c).

3. Distribution of Residual Pore Pressure after Rapid-Drawdown of the Reservoir

(1) Pore pressure and residual strength after rapid-drawdown.

Among the various data of earth dam failure, sloughing of upstream slope due to rapid-drawdown of the reservoir is one of the most predominant causes, whereof many old-typed French earth dams have been destroyed[22]. This type of failure is not disastrous generally, but it is costly for restoration.

In this case, the reason why the earth embankment becomes unstable is that, in consequence of having discharged the water load, the residual strength is being decreased remarkably, by the decrease of total normal stresses and of the insufficient decrease of the pore pressure that should be accompanied with that of the former.

The author draws Fig. 8 to explain the mechanism of this earth dam

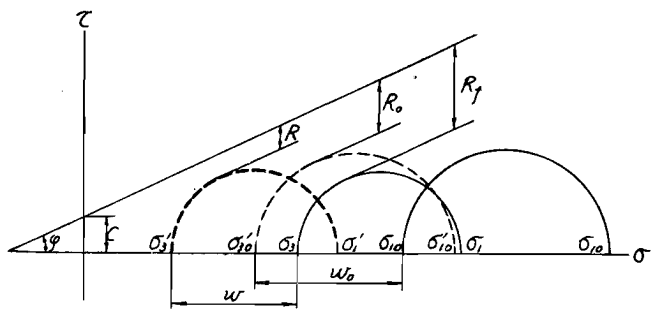

Fig. 8 Mohr's stress circles and residual strengths in the embankment before and after drawdown.

failure. This figure shows Mohr's circles at any point in a soil element near the upstrem slope, from which the position of stress circle and the residual strength just after drawdown and in the following period are cleared, referring Table 2.

As is shown in Fig. 8, at the instance of rapid-drawdown, it is known that the residual strength in the embankment decreases, resulting that the struc-

Table 2 Relation between stresses, pore pressure and residual strength in the earth embankment before and after drawdown.

	Before drawdown	Just after drawdown	After lapse
Total stresses	σ_{10}, σ_{30}	σ_1, σ_3	σ_1, σ_3
Pore pressure	w_0	w	$w\rightarrow 0$
Effective stresses	σ_{10}', σ_{30}'	σ_1', σ_3'	$\sigma_1'\rightarrow\sigma_1$, $\sigma_3'\rightarrow\sigma_3$
Residual strength	R_0	$R(<R_0)$	$R\rightarrow R_f$

ture approaches to its dangerous state.

Though the intensity of the residual pore pressure is variable by the geometry of the embankment, physical properties of the material and the degree of compaction, it is possible to express these factors by a unique coefficient. The residual pore pressure just after rapid-drawdown is given in the following form, referring Fig. 9 :

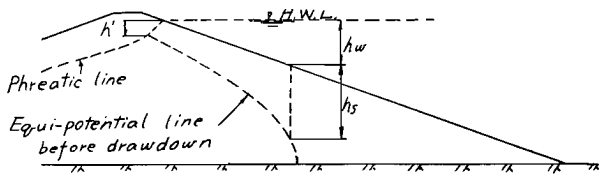

Fig. 9 h_s, h_w and h' before drawdown.

$$w=\gamma_w\{h_s+h_w(1-\bar{B})-h'\} \qquad \cdots\cdots\cdots\cdots(12)$$

As is seen from Eq. (12), the smaller the value of the overall pore pressure coefficient $\bar{B}$ is, the larger the pore pressure w remains, and the embankment becomes unstable, whereas from Eq. (6) when A=1, $\bar{B}=B=1$ and for $A<1$, $\bar{B}>B$, resulting $\bar{B}>1$. As a safe side, taking $\bar{B}=1$ follows :

$$w=\gamma_w(h_s-h')\,. \qquad \cdots\cdots\cdots\cdots(13)$$

This gives the residual pore pressure of the worst case. It should be noted that in this case, B is less than unity but, as its magnitude depends on the sign of the change in stress, the values of A and B measured in the conventional undrained test with increasing principal stresses as is described in **2. (5)** are not applicable.

In order to estimate the residual pore pressure after rapid-drawdown of the reservoir from Eq. (13), the potential drop h' in Fig. 9 should be known

at each situation in the earth embankment, drawing the flow-net of steady seepage flow at full reservoir. There are various means of establishing the flow-net in the embankment, among which the author applies the relaxation method, which has been developed by Southwell[23], to Fresno Dam described in the preceding article. Fig. 10 illustrates the distribution of residual pore pressure

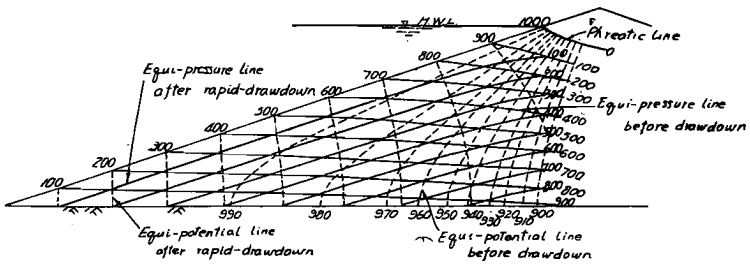

Fig. 10 Distribution of residual pore pressure in the upstream region of the embankment of 1 3-slope just after rapid-drawdown.

in the upstream region just after rapid-drawdown calculated by Eq. (13). In the figure, equi-potential lines and equi-pressure lines before drawdown and equi-potential lines after drawdown are marked, in connection with equi-pressure lines after drawdown under consideration.

From the above calculation it is known that, at the instance just after rapid-drawdown of the reservoir, in spite of the remarkable decrease of total normal stresses in the upstream region, pretty large amount of the residual pore pressure exists, making the reserve strength in the embankment extremely small. To prevent the dam failure by this effect, it can be known that, as well as the installation of an adequate filter-drain at the toe of upstream slope to decrease the pore pressure, the definition of a permissible speed of the drawdown of the water level, or the limitation of partial discharge instead of integral discharge is an important factor in the design and the hydraulic treatment of the earth embankment[24]

(2) Stability computation.

For example, the stability computation after rapid-drawdown of the reservoir for an earth embankment is performed, which has a symmetrical section of 1 : 3-slope shown in Fig. 3. From the above-mentioned consideration, the overall pore pressure coefficient $\bar{B}$ corresponding to the stress change of drawdown is adopted $\bar{B}=1$ for the sake of safety. Fig. 11(a), (b) shows the dis-

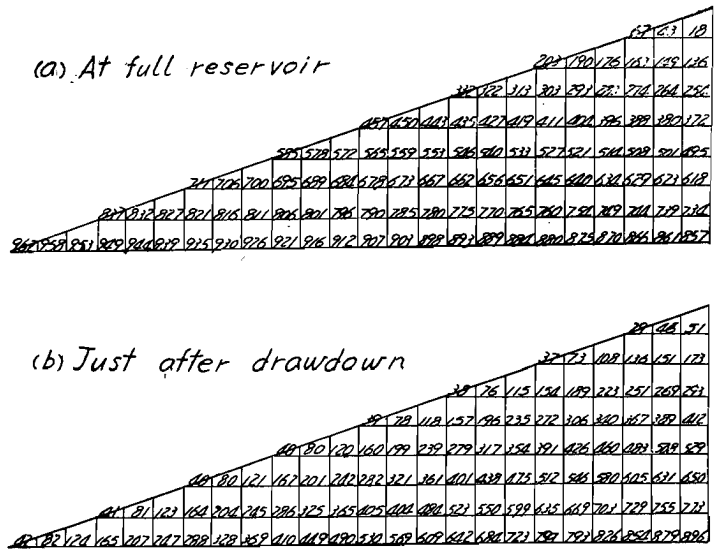

Fig. 11 Distribution of actual pore pressure in the embankment of 1 3-slope ; (a) at full reservoir and (b) just after drawdown.

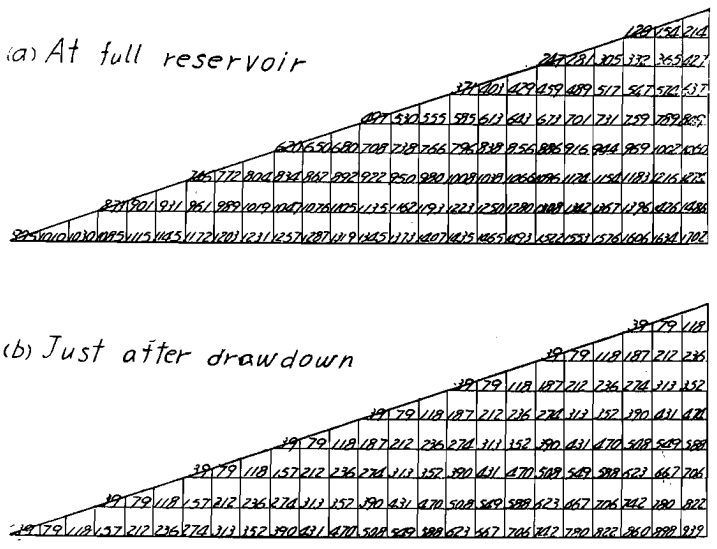

Fig. 12 Distribution of permissible pore pressure in the embankment of 1 : 3-slope ; (a) at full reservoir and (b) just after drawdown.

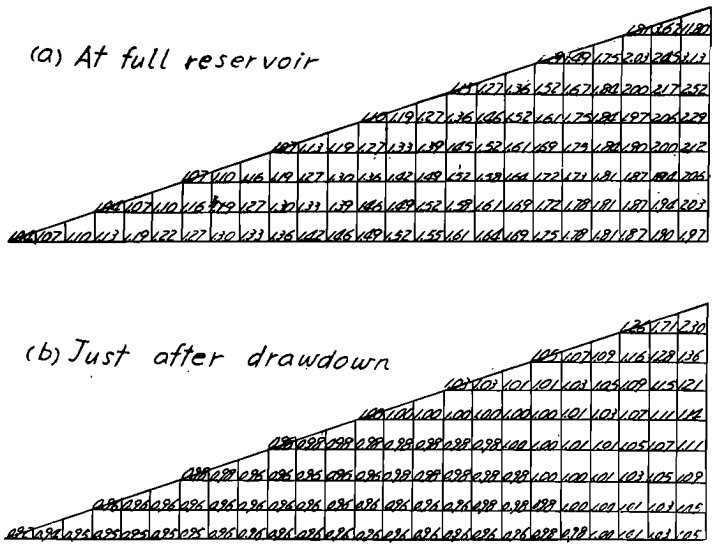

Fig. 13 Distribution of factor of safety in the embankment of 1 3-slope ; (a) at full reservoir and (b) just after drawdown.

tribution of the pore pressure before and just after drawdown, respectively, copying from Fig. 10. Fig. 12(a), (b) is the distribution of the permissible pore pressure calculated from the residual shearing resistance, using $\tan\varphi=0.5$ ($\varphi=26°34'$) and $C=0$ ($K=1.0$ for (a) and $K=0.7$ for (b)). In Fig. 13(a), (b), the factor of safety of the embankment before and after drawdown is shown, respectively, which represents the ratio of the permissible pore pressure in Fig. 12 to the actual pore pressure in Fig. 11.

As is seen from calculating example, the factor of safety at the upstream toe just after drawdown decreases extremely, resulting the danger of sloughing to be approached. Therefore, the stability of the embankment against rapid-drawdown should be established by the installation of the filter-drain at this part, or by the reasonable treatment of discharging the reservoir.

4. Conclusion

In the present part of this paper, among the effects of the pore pressure on the stability of earth embankments, an analytical study is performed for the pore pressure coming into existence due to the consolidation of fill material during construction, and for the residual pore pressure after rapid-drawdown

of the reservoir, respectively. In the result, it is known that such pore pressures have a serious effect on the stability of the earth embankment, according to the numerical calculations for the above both criteria. And the conclusion is that, as well as the design of the adequate drainage to accelerate the dissipation of the pore pressure, the critical permissible pore pressure must be checked in the execution control of earth embankment and the treatment of drawdown of the reservoir.

Acknowledgments

The author earnestly wishes to express his appreciation to Prof. Sakurō Murayama for his constant instruction in performing this study. Thanks are also due to the Grant in Aid for Scientific Research of the Ministry of Education.

References

1) R. G. Hennes : Discussion to "Stability of Granular Materials", Trans. Am. Soc. Civil Engrs., Vol. 108, 1943, pp. 64–65.
2) Z. Anzo : Pressure Exerted by Granular or Pulverulent Material, Memoirs of the Faculty of Eng., Kyūshū Univ., Vol. 7, 1933, pp. 89–143.
3) F. Jonson : Calculation of the Stability of Earth Dams, Trans. 2nd Congr. on Large Dams, Vol. 4, 1936, pp. 463–480.
4) R. E. Glover and F. E. Cornwell Stability of Granular Materials, Trans. Am. Soc. Civil Engrs., Vol. 108, 1943, pp. 46–63.
5) S. V. Benscoter : Discussion to "Stability of Granular Materials", Trans. Am. Soc. Civil Engrs., Vol. 108, 1943, pp. 65–69.
6) D. P. Krynine Discussion to "Stability of Granular Materials", Trans. Am. Soc. Civil Engrs., Vol. 108, 1943, pp. 72–78.
7) J. H. A. Brahtz Brahtz Method of Stability Analysis, Treatise on Dams, Chapt. 8, pp. 101–170.
8) J. Ohde : Druckverteilung in und unter Erddämmen, Wasserwirtschaft–Wassertechnik, Vol. 3, 1953, pp. 248–252.
9) J. Ohde Zur Erddruck–Lehre, Bautechnik, Vol. 29, 1952, pp. 219–224.
10) K. Terzaghi Theoretical Soil Mechanics, 1948, pp. 177–181.
11) K. Akai : On the Local Failure of the Downstream Slope of Embankments Due to the Percolating Flow, Trans. Japan Soc. Civil Engrs., No. 36, 1956, pp. 44–49 (in Japanese).
12) S. Murayama and K. Akai : An Experimental Research on the Local Failure of the Downstream Slope of Embankments and the Preventive Methods, Bulletin of Disaster Prevention Research Institute, Kyōto Univ., Memorial Issue of the 5th Anniversary, 1956, pp. 59–66 (in Japanese).
13) S. Murayama and K. Akai : Failure of the Embankment Foundation, Bulletin of Disaster Prevention Research Institute, Kyōto Univ., No. 8, 1954, pp. 1–15.
14) W. W. Daehn and J. W. Hilf : Implications of Pore Pressure in Design and Construction of Rolled Earth Dams, Trans. 4th Congr. on Large Dams, Pt. 2, 1951, pp. 259–283.
15) A. Rufenacht : Pore Pressure Assumptions for Stability Studies of Earth Dams, Proc. 2nd Intern. Conf. Soil Mech. and Foundation Eng., Vol. 3, 1948, pp. 230–233.
16) J. W. Hilf Estimating Construction Pore Pressures in Rolled Earth Dams, Proc. 2nd Intern. Conf. Soil Mech. and Foundation Eng., Vol. 3, 1948, pp. 234–240.
17) K. Terzaghi and O. K. Fröhlich Theorie der Setzung von Tonschichten, 1936, pp. 43–45, 91–96.
18) R. G. Olsson Approximate Solution of the Progress of Consolidation in a Sediment, Proc. 3rd Intern. Conf. Soil Mech. and Foundation Eng., Vol. 1, 1953,pp. 38–42.
19) R. E. Gilson and P. Lumb : Numerical Solution of Some Problems in the Consolidation of Clay, Proc. Inst. Civil Engrs., Pt. 1, Vol. 2, 1953, pp. 182–198.
20) A. W. Skempton The Pore–Pressure Coefficients A and B, Géotechnique, Vol. 4, 1954, pp. 143–147.
21) A. W. Bishop The Use of Pore–Pressure Coefficients in Practice, Géotechnique, Vol. 4, 1954, pp. 148–152.

22) A. Mayer : Characteristics of Materials Used in Earth Dam Construction —— Stability of Earth Dams in Cases of Reservoir Discharge, Trans. 2nd Congr. on Large Dams, Vol. 4, 1936, pp. 295–330.
23) R.V. Southwell Relaxation Methods in Theoretical Physics, 1946, pp. 201–212.
24) O. K. Fröhlich On the Danger of Sliding of the Upstream Embankment of an Earth Dam, Caused by Complete or Partial Discharge of the Reservoir, Trans. 4th Congr. on Large Dams, Pt. 2, 1951, pp. 329–342.

Publications of the Disaster Prevention Research Institute

The Disaster Prevention Research Institute publishes reports of the research results in the form of bulletins. Publications not out of print may be obtained free of charge upon request to the Director, Disaster Prevention Research Institute, Kyoto University, Kyoto, Japan.

Bulletins :

No. 1 On the Propagation of Flood Waves by Shoitiro Hayami, 1951.
No. 2 On the Effect of Sand Storm in Controlling the Mouth of the Kiku River by Tojiro Ishihara and Yuichi Iwagaki, 1952.
No. 3 Observation of Tidal Strain of the Earth (Part I) by Kenzo Sassa, Izuo Ozawa and Soji Yoshikawa. And Observation of Tidal Strain of the Earth by the Extensometer (Part II) by Izuo Ozawa, 1952.
No. 4 Earthquake Damages and Elastic Properties of the Ground by Ryo Tanabashi and Hatsuo Ishizaki, 1953.
No. 5 Some Studies on Beach Erosions by Shoitiro Hayami, Tojiro Ishihara and Yuichi Iwagaki, 1953.
No. 6 Study on Some Phenomena Foretelling the Occurrence of Destructive Earthquakes by Eiichi Nishimura, 1953.
No. 7 Vibration Problems of Skyscraper. Destructive Element of Seismic Waves for Structures by Ryo Tanabashi, Takuzi Kobori and Kiyoshi Kaneta, 1954.
No. 8 Studies on the Failure and the Settlement of Foundations by Sakurō Murayama, 1954.
No. 9 Experimental Studies on Meteorological Tsunamis Traveling up the Rivers and Canals in Osaka City by Shoitiro Hayami, Katsumasa Yano, Shohei Adachi and Hideaki Kunishi, 1955.
No.10 Fundamental Studies on the Runoff Analysis by Characteristics by Yuichi Iwagaki, 1955.
No.11 Fundamental Considerations on the Earthquake Resistant Properties of the Earth Dam by Motohiro Hatanaka, 1955.
No.12 The Effect of the Moisture Content on the Strength of an Alluvial Clay by Sakurō Murayama, Kōichi Akai and Tōru Shibata, 1955.
No.13 On Phenomena Forerunning Earthquakes by Kenzo Sassa and Eiichi Nishimura, 1956.
No.14 A Theoretical Study on Differential Settlements of Structures by Yoshitsura Yokoo and Kunio Yamagata, 1956.
No.15 Study on Elastic Strain of the Ground in Earth Tides by Izuo Ozawa, 1957.
No.16 Consideration on the Mechanism of Structural Cracking of Reinforced Concrete Buildings due to Concrete Shrinkage by Yoshitsura Yokoo and S. Tsunoda. 1957.
No.17 On the Stress Analysis and the Stability Computation of Earth Embankments by Kōichi Akai, 1957.

Bulletin No. 17 Published March, 1957

昭和 32 年 3 月 20 日 印 刷
昭和 32 年 3 月 25 日 発 行
編輯兼発行者 京都大学防災研究所
印刷者 山 代 多 三 郎
京都市上京區寺之内通小川西入
印刷所 山代印刷株式会社